Electrochemical Materials and Technologies

REVIEW

Electrochemical Materials and Technologies

eISSN: 2949-0561

Cite this: Electrochem. Mater. Technol. 2 (2023) 20232012

Received: 29 March 2023
Accepted: 16 May 2023
Published online: 22 May 2023

DOI: 10.15826/elmattech.2023.2.012

Molecular dynamic study of the applicability of silicene lithium ion battery anodes: A review

Alexander Galashev [ab] *

Lithium-ion batteries (LIBs) are the main energy storage devices that have found wide application in the electrical, electronics, automotive and even aerospace industries. In practical applications, silicene has been put forward as an active anode material for LIBs. This is facilitated by its high theoretical capacitance, strength, and small volume change during lithiation. Thin-film materials containing two-layer silicene and intended for use in the LIB anode have been studied by the method of classical molecular dynamics. Among the important characteristics obtained is the fillability of the silicene anode (under the influence of an electric field), which was determined depending on the type of vacancy defects in silicene and the type of substrate used. Both metallic (Ag, Ni, Cu, Al) and non-metallic (graphite, silicon carbide) substrates are considered. The behavior of the self-diffusion coefficient of intercalated lithium atoms in a silicene channel as it is filled has been studied. Based on the construction of Voronoi polyhedra, the packing of lithium atoms and the state of the walls in the channel has been studied in detail. The change in the shape of silicene sheets, as well as the stresses in them caused by lithium intercalation, are analyzed. It has been established that two-layer silicene with monovacancies on a nickel substrate is the most optimal variant of the anode material. The results of this work may be useful in the development of new anode materials for new generation LIBs.

keywords: anode, molecular dynamics, self-diffusion, silicene, stress, structure

1. Introduction

Currently, lithium-ion batteries (LIBs) have found applications not only in portable electronics, but also in electric cars, power tools, medical devices, smart watches, drones, satellites, and utility-scale storage. Each specific application requires appropriate battery sizes and designs, as well as charging capacity and speed. The duration of modern batteries is up to one year, and in some cases they can function for several years. In the absence of stable electrolytes, it was possible to achieve lithiation of the anodes (negative electrodes) to potentials close to metallic lithium. The decomposition of the electrolyte is retarded by the formation of a solid electrolyte interfacial layer (SEI). The aluminum current collector on the cathode side resists corrosion for a sufficiently long time, also due to the formation of a stable passivation layer. Cathode materials successfully withstand the mechanical stresses of repeated volume changes associated with the removal and introduction of lithium. The used electrode materials actually work on the verge of their functional limits. This means that an even greater removal of lithium from the cathode will cause a loss of oxygen, i.e. lead to irreversible structural transformations. At the same time, an even greater filling of the anode becomes impossible due to the complete absence of vacancies in the lattice, which should be filled with lithium ions. Surface coatings, electrolyte additives, and morphology optimization allow for thinner separators and current collectors, ultimately allowing for higher voltages.

New electrode materials are regularly researched. However, their commercialization is possible only if they are scalable. In addition, it is necessary to ensure that the volumetric and gravimetric energy densities reflect the

a: Institute of High Temperature Electrochemistry, Ural Branch of Russian Academy of Sciences, Ekaterinburg 620990, Russia
b: Institute of Chemical Engineering, Ural Federal University, Ekaterinburg 620009, Russia

* Corresponding author: galashev@ihte.uran.ru

energy density of the electrode, and not of the material. In other words, the performance of an electrode containing enough active material to realize the required energy density must be ensured. In connection with this requirement, we can only talk about a limited number of new classes of battery materials. Among the new materials, one can mention carbon phosphates, which are identified as a new type of mineral structure [1]. At the same time, despite the appearance of a number of metastable structures, their identification is not at the proper level. First of all, this concerns the identification of resistance to cycling, as well as to structural reorganizations. The structure can be predicted theoretically. But the problem is whether such structures can be synthesized and how [2].

For the normal functioning of small-sized devices (microsensors, drug delivery microsystems, micromachines), it is necessary to create high peak currents in a limited volume [3, 4]. This can be done using a self-contained power source with a stable current, such as a lithium-ion battery. Until recently, the microbatteries had a thin-film two-dimensional (2D) architecture suitable for industrial production [5]. However, as it turned out, it is difficult to achieve high power and energy density for 2D structures with a small size. It is possible to increase the power and energy density without a significant increase in volume by switching to three-dimensional (3D) microbatteries [6]. The design of these batteries makes it possible to increase the proportion of active material in LIB.

Rechargeable microbatteries have the same working principle as standard LIBs. Charge carriers (lithium ions) passing between the cathode and anode generate electrical energy. The cathode and anode are separated by a liquid or solid electrolyte. The main difference between microbatteries and standard LIBs is their small volume, which can be less than 0.01 cm^3. Due to the small volume, the geometry and materials of the electrodes are critical to the power and density of microbatteries [7].

To reduce the size of traditional LIBs, inactive materials such as separators must be removed. In addition, high energy efficiency can be achieved by the introduction of new electrodes and electrolytes. Although commercial liquid electrolytes have high ionic conductivity, they are not safe due to the risk of leakage [8]. Solid electrolytes are being actively developed for microbatteries at the present time. The main problem is their unsatisfactory bulk and interfacial characteristics [9, 10]. A solid electrolyte for a microbattery should have: 1) high ionic conductivity (10^{-4} $S{\cdot}m^{-1}$) at room temperature [11], significantly lower (than ionic conductivity) electronic conductivity [12], high electrochemical and thermal resistance to electrode materials [13], resistance to the formation of lithium dendrites [14], low cost and toxicity, ease of synthesis, and the possibility of production on a large scale.

There are two main groups of solid electrolytes: polymer-based electrolytes and inorganic electrolytes. The first type achieves high ionic conductivity (up to 10^{-4} $S{\cdot}cm^{-1}$), is easy to manufacture, has flexibility, and is able to limit the change in the volume of an electrode such as Si [15, 16]. The second type of electrolyte is divided according to the structure of the material into crystalline and glass. For example, perovskites and garnet-type electrolytes are classified as crystalline, while lithium phosphate-containing compounds are characterized as glassy [17, 18].

Improving the performance of microbatteries is achieved by optimizing the architecture of the 3D batteries, which can be done automatically with finite element modeling. To achieve this goal, an automatic geometry generator and a performance simulator [19] are used. For example, a quick estimate of the internal resistance that relates the power and energy density can be made using a 3D porous electrode model that mimics a transmission line model.In the stationary mode of operation of the microbattery, modeled by the finite element method, ion transport in the electrolyte was described by the Nernst-Planck equation, and electrode potentials – by Ohm's law [20]. It has been shown that the polymer electrolyte used in the microbattery is able to provide more uniform electrochemical activity, but is not able to withstand such high currents as liquid electrolytes.

Finite element modeling makes it possible to reveal a picture of some phenomena occurring over a time interval approaching the real time interval. This determines the main merit of such calculations. However, the tool in such studies is a macroscopic description of systems and the phenomena occurring in them. Such an approach is not always justified when the events associated with the individual behavior of atoms and ions that carry out transport and directly interact with the electrode materials come to the fore. The study of phenomena occurring in operating LIBs at the atomic level is not less important than the numerical solution of problems related to the functioning of chemical energy sources using the finite element method. At present, when a huge amount of experimental research is being carried out related to the development of new high-performance LIBs, the molecular dynamics study of the selection of electrode materials for them is especially important.

Among all potential LIBs anodes, silicon seems to be the most suitable candidate to replace graphite. The reason for this is the following circumstances: 1) Si has the

highest gravimetric capacity among other candidates, with complete lithiation, there are 4.4 Li atoms per 1 Si atom [21]; 2) the average discharge voltage that the Si anode exhibits is 0.4 V, thus there can be a good balance between the open circuit voltage and the absence of an unfavorable lithium coating process [22]; 3) Si is widely distributed in the Earth's crust, so it is potentially cheap, environmentally friendly, and non-toxic [23].

The silicon analog of graphene, silicene, is built in the form of a hexagonal grid of silicon atoms. This two-dimensional (2D) material is of interest both in terms of fundamental research and applications in the electronics industry. According to theoretical calculations, many of the physical properties of graphene are also characteristic of silicene. In particular, silicene should have massless Dirac fermions, the quantum spin Hall effect should manifest itself in it, and there is the possibility of superconductivity in silicene [24]. The bonds between silicon atoms in silicene are formed due to the formation of a mixed sp^2/sp^3 hybridization [25]. Silicene exhibits a strong interaction with a metal substrate, which can significantly change the remarkable electronic properties of this two-dimensional material [26]. This, in particular, was found in the epitaxial silicene layer on the Ag(111) surface [27]. However, if the interaction of silicene with the substrate is much weaker, then it can retain the important properties of free-standing silicene.

Silicene, which has a structure with low buckles and partial sp^3 hybridization of silicon atomic orbitals, cannot exfoliate from bulk silicon. The main method for the synthesis of silicene is an epitaxial growth on solid surfaces. Silicene was obtained on metal surfaces (Ag, Au, Ir) [28–30]. In addition, silicene was grown on ZrB_2 thin films located on Si wafers [31], as well as on ZrC [32]. In addition, silicene was obtained by molecular beam epitaxy on bulk MoS_2 [33]. A silicon monolayer can be grown on highly oriented pyrolytic graphite at room temperature [34]. Silicene covered up to 80 % of the entire surface, but along with it, small silicon clusters up to 1 nm high were also formed on the surface. DFT calculations showed that the Dirac cone is present in the silicene on the graphite substrate.

Typically, the substrates on which silicene is grown correspond to single-crystal surfaces of the material. They are prepared in an ultra-high vacuum environment (base pressure 10^{-10} Torr) to obtain atomically well-defined surfaces of at least a few hundred square nanometers. Still, silver surfaces are most commonly used as substrates. This is due to the good agreement between the lattice constants of Si and Ag, which are in the ratio ¾, as well as the insignificant miscibility of the Si and Ag solid phases at temperatures below ~1070 K. The high sensitivity of silicene to the chemical environment can be used to tune its electronic properties through molecular adsorption.

A wide variety of battery designs suitable for a wide range of operating conditions at low cost can be obtained from simulation combined with experimental verification. It was shown that the complete lithiation of silicene results in the transformation of the band structure of the zero semiconductor into the structure of a semiconductor with a band gap of 0.37 eV [35]. Graphene otherwise behaves during lithiation, turning into a metal [36]. In addition, after delithiation, silicene largely restores its state. This distinguishes it from crystalline silicon, which is destroyed during cycling [37]. Regardless of the concentration of adsorbed Li atoms, lithium easily diffuses on silicene, overcoming a low energy barrier [38]. A detailed study of the physical properties of silicene shows that it is a suitable material for lithium-ion battery anodes [39].

Improving the performance of LIBs continues. Many works are aimed at increasing the energy density while maintaining service life and safety. This review highlights the main studies performed by the method of classical molecular dynamics, which touch upon the design of this thin film silicene anode, the dependence of the functional characteristics of the anode on the defectiveness of silicene, the size of the gap between silicene sheets, the type of substrate used to support silicene, the structure of the packings of adsorbed lithium atoms, the mobility of these atoms in the course of intercalation and deintercalation, stress in silicene sheets due to the incorporation of lithium into the channel formed by them, and some other issues.

2. Materials and methods

In LIBs, chemical energy is converted into electrical energy during the discharge process, i.e. when lithium ions move from the anode to the cathode. The lithium ions in the battery are electronically isolated. Figure 1 shows a schematic of a liquid electrolyte lithium-ion battery. A liquid electrolyte generally has a higher ionic conductivity than a solid electrolyte. However, solid electrolyte batteries are safer than liquid electrolyte batteries. Silicene is more often obtained on a metal substrate from which it is difficult to separate. The use of silicene as an anode material in this case involves the isolation of the metal substrate from an external electrical circuit. The design of the electrode must also provide for the isolation of the metal substrate from the electrolyte. As a result, contact with the chain should be carried out only through silicene.

As the battery functions, a SEI is formed at its negative electrode. SEI education has both positive and negative effects. The positive effect is that SEI protects the

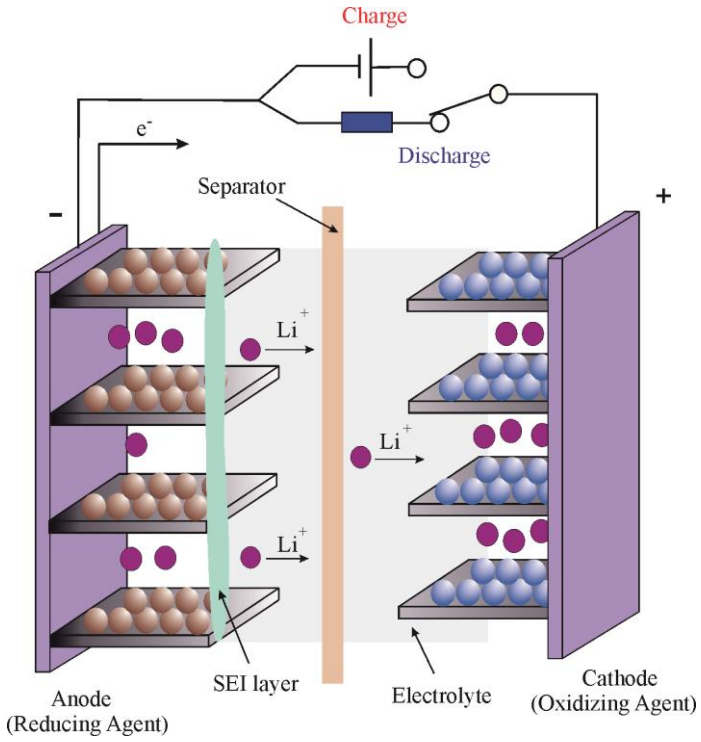

Figure 1 Schematic of a typical state-of-art lithium-ion battery.

electrode against solvent decomposition at large negative voltage. However, the gradual thickening of the SEI layer, associated with irreversible electrochemical processes, leads to a gradual decrease in battery capacity. At present, a detailed picture of the adsorption and desorption of lithium on silicene sheets located on both metal and non-metal substrates can be displayed by computer simulation.

Such calculations were performed by the classical molecular dynamics (MD) method. Interactions between Si atoms in silicene were described by the Tersoff potential [40], and interactions between Si atoms belonging to different silicene sheets were represented by the Morse potential [41]. The Morse potential has also been used to describe the Li-Li, Li-Si, Li-Me and Si-Me interactions, where Me = Ag, Ni, Cu, Al.

A silicene channel located on either a metallic (Ag, Ni, Cu, Al) or a nonmetallic (graphite, SiC) substrate served as a model for performing molecular dynamics calculations. The channel was formed by two parallel sheets of silicene. The channel gap varied from 0.24 to 0.85 nm depending on the purpose of the work [42]. However, in most calculations, the channel gap was 0.75 nm [41]. It is with this gap that a lithium ion entering the channel could migrate for a long time (up to 0.1 ns) along it when an external electric field with a strength of 10^3–10^4 V/m was applied [43]. A close value of the electric field (when creating a working voltage of 1.5 V) is achieved in LIB, when a LiPON film ~30 μm thickness is used as a solid electrolyte [38]. In the works discussed here, the minimum value of the electric field strength was selected (from the range of 10^3–10^5 V/m), which ensured the intercalation or deintercalation process. Similar calculations with different electric field strengths were not performed. The value of the channel gap must be consistent with the magnitude of the electric field strength under the action of which lithium ions can fill the silicene channel. The Li^+ ion entering the channel had an electric charge for a short time (10 ps), and then received one electron from a negatively charged electrode (represented by a silicene channel) and turned into a neutral atom. In this state, it remained all the main time spent in the channel. Thus, neutral Li atoms were accumulated in the channel. To free the channel from lithium, a constant reverse electric field has been applied. The strength of this field was usually an order of magnitude higher than the field strength at which the intercalation was carried out. During deintercalation, atoms in the reverse order of entering the channel, or randomly selected, again acquired an electric charge (losing an electron). The time interval after which any Li atom received an electric charge was also 10 ps. The emerging ions left the silicene channel.

Silicene had a floral structure, the unit cell which contained 18 Si atoms, six atoms of which rose above the basal plane by the distance of 0.064 nm (Figure 2). It is this structure that was identified in the preparation of silicene on the Ag (111) substrate [44]. The buckled honeycomb lattice of silicene has been confirmed by various experimental methods including non-contact atomic force microscopy, scanning tunneling microscopy, angle-resolved photoelectron spectroscopy, and low-energy electron diffraction [44]. In addition, such a

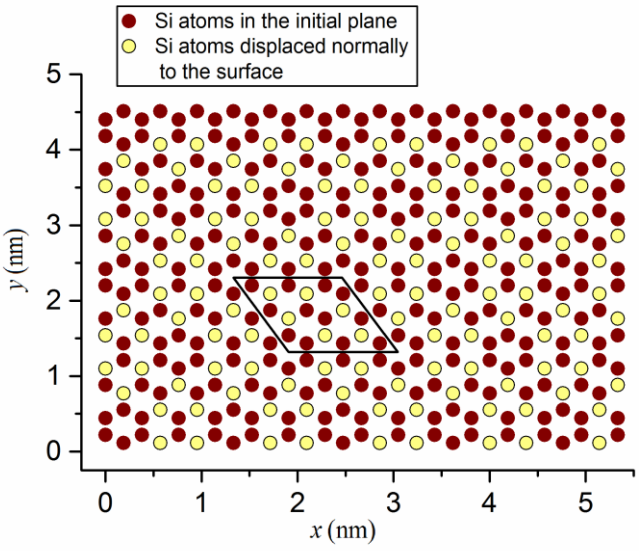

Figure 2 Top view of the silicene structure at the initial instant; an outline shows a surface cell unit of the silicene sheet.

structure occupies the largest part of the surface of epitaxial silicene on the substrate Ag(111) [27, 45].

The mutual arrangement of the parallel silicene sheets corresponded to the Bernal stacking (ABAB...), as well as for graphene sheets in graphite [46]. To preserve the morphology of the silicene sheets and avoid their rotation during simulation, the edges of the sheets were fixed. A short-range force field acted at the edges of the channel during intercalation, which prevented the release of lithium atoms from it [47]. Flat channels formed both by sheets of perfect and defective silicene were studied. A sheet of perfect silicene was usually formed by 300 Si atoms. The defects were polyvacancies, which were distributed approximately evenly over the silicene sheets. Mono-, bi-, tri-, and hexavacancies were considered. Real silicene obtained on both metallic and non-metallic substrates contains defects. Defects can be initiated by a mismatch between the lattice parameters of the crystalline substrate and silicene, and also arise during the growth of Si clusters from different centers. In silicene grown on an Ag(111) substrate, mono- and bivacancies are present in the greatest amount. Their estimated number is $4.4 \cdot 10^{13}$ cm^{-2} and $5.0 \cdot 10^{13}$ cm^{-2}, for mono- and bivacancies, respectively [48]. According to this estimate, there is one defect for every 2 nm^2. The presence of defects reduces the stability of silicene. The silicene channel was filled with lithium until all Li^+ ions got into the channel. If at least one injected ion left the channel within 10 ps, the calculations were terminated.

In what follows, we will refer to the silicene (graphene) as a two-dimensional silicon (carbon) material with a hexagonal cell structure , and thin films as a two-dimensional silicon (carbon) material having the structure of bulk crystalline silicon (graphite). Only crystalline silicon films with a cubic face-centered lattice of the diamond type are considered.

The molecular dynamics calculations presented in this review were performed at a temperature of 300 K, which distinguishes them from conventional DFT calculations, the results of which refer to a temperature of 0 K. The data obtained in MD calculations, refer to the pressure range from 0.1 to 10 MPa.

The detailed packing structure of lithium atoms in the channel can be examined by constructing Voronoi polyhedra (VP). In this case, structural characteristics are obtained, expressed in terms of topological and metric properties of Voronoi polyhedra. The topological characteristics include the distribution of polyhedra over the number of faces (n distribution) and the distribution of faces over the number of sides (m distribution). The metric characteristic is the distribution of the angles ϑ formed by the segments connecting the center VP (the vertex of the angle ϑ) with all possible pairs of geometric neighbors that give VP faces. The probability of finding the considered number of nearest geometric neighbors is reflected by the n distribution, and the probability of finding m-link rings visible from the center of VP along the nearest neighbor directions is given by the m distribution. The angular distribution reflects the most characteristic central angles (angles ϑ), under which the nearest geometric neighbors are located.

To calculate stresses arising in silicene, every sheet is divided into elementary areas. The stresses $\sigma_{u\alpha}(l)$ caused by forces in the α (= x, y, z) direction are calculated for each l-th area with u orientation. In these calculations the products of projections of atomic velocities and projections of forces f_{ij}^{α} acting on the l-th area from the side of other atoms are used if corresponding conditions are satisfied [49]

$$\sigma_{u\alpha}(l) = \left\langle \sum_{i}^{k} \frac{1}{\Omega} \left(m v_u^i v_\alpha^i \right) \right\rangle + \frac{1}{S_l} \left\langle \sum_{i}^{k} \sum_{j \neq i}^{(u_i \le u, u_j \ge u)} \left(f_{ij}^{\alpha} \right) \right\rangle. \qquad (1)$$

Here k is the number of atoms on the l-th area, Ω is the volume per atom, m is the atom mass, v_α^i is the α-projection of the i-th atom velocity, and S_l is the l-th area. The conditions of summation over j in the last sum of expression (1) are reflected in both the lower and upper indexes of the sum; the force arising during the interaction of atoms i and j passes through the l-th area; u_i is the current coordinate of atom i; in the upper bound of the sum, u is the coordinate of the point of contact of the straight line passing through the centers of atoms i and j with the l-th area.

The calculations were performed using the LAMMPS program [50].

3. Anode material in the form of silicene and silicene on a metal substrate

3.1. Lithium intercalation and deintercalation in a freestanding silicene channel

Back in 1994, based on density functional theory (DFT) calculations, it was shown that a single atom-thick sheet of Si or Ge atoms in a curved honeycomb structure can be energetically stable [51]. However, the convincing experimentally confirmed growth of silicene on a single-crystal Ag (111) silver substrate was carried out in [52], only 18 years later. In this work, using scanning tunneling microscopy, a beautiful "flower pattern" of the canonical silicene phase could be seen on a silver plate. Silicene, a

two-dimensional material formed from Si atoms, should be characterized by adsorption properties similar to those of its bulk (three-dimensional) analogue, i.e. silicon. When lithium is intercalated into bulk silicon, a record theoretical gravimetric capacity (4200 mA·h·g^{-1}) can be achieved, which is more than an order of magnitude greater than the capacity of graphite (272 mA·h·g^{-1}) [53]. However, when lithium is introduced into bulk silicon, an extremely large increase in volume (up to 300 %) of crystalline silicon occurs [54]. After deintercalation, this material does not return to its original state, and after several cycles it cracks and crumbles. In this case, the electrode is destroyed, and the battery fails. A DFT study showed that a fully lithiated silicene sheet acquires the most stable thermodynamic state [39]. Through the theoretical studies of Tritsaris et al. [35] found that the diffusion of lithium on silicene occurs with low energy barriers (less than 0.6 eV). In addition, after complete lithiation, single-layer and double-layer silicene increases in volume by 13 % and 24 %, respectively. The absence of visible damage after delithiation was the basis for the assertion that silicene is a promising anode material with a high energy density and a long service life.

Before studying the filling of a silicene channel located on any of the substrates with lithium, a free-standing perfect silicene channel was filled with lithium in the molecular dynamics model [55, 56]. Lithium ions entered the channel under the action of a constant electric field with a strength of 10^3 V/m. Since there was no substrate, it was important to trace the shape of the channel during lithium intercalation and deintercalation. The channel gap was 0.75 nm. The gap size was selected empirically. It was important that, at a given electric field, the Li^+ ion, on the one hand, could move quite freely through the channel, and, on the other hand, linger in the channel for a time interval at least an order of magnitude greater than the interval (10 ps) separating the launches of ions into the channel during intercalation. These requirements were fully met by a channel with a gap of 0.75 nm. Si atoms forming the perimeter of silicene sheets were fixed in their positions during cycling. This ensured successful intercalation and deintercalation processes.

It is of interest to compare the capacitances of real and calculated anodes in which silicon is present. The work [57] describes an anode made of a multilayer structure containing graphene oxide, carbon nanotubes, and silicon nanoparticles filling them. The anode material showed a capacity of 1211.15 mAh·g^{-1} after 100 cycles. An anode for microbatteries was fabricated by depositing graphene on floral silicene by chemical vapor deposition (CVD) [58]. Floral silicene was created by reducing silicon dioxide with magnesium. Within 500 cycles, the specific capacity of this combined anode was more than five times higher than the theoretical capacity of graphite.

DFT studies have shown that the calculated capacity of lithium-filled silicene anodes is limited by their mechanical stability [59]. So the theoretical specific capacity of a single-layer silicene anode is estimated as 1196 mAh/g [60]. For a two-layer silicene anode, it has a value of 1384 mAh/g [61].

In this computer experiment, a mixed method of filling the channel with lithium was used. At first, lithium ions were launched into the channel singly, but when the number of Li atoms in the channel reached 28, ions were launched into the channel in pairs while maintaining the same time interval between launches. As a result, 38 Li atoms were introduced into the channel. Attempts to introduce more atoms were unsuccessful. As a result of the intercalation, the channel acquired a convex shape; the silicene sheets turned out to be curved outwards (Figure 3). This resulted in a 26 % increase in channel volume. The intercalation of the first 13 Li atoms leads to the formation of a lithium cluster in the central part of the channel, which can be observed in the inset at the top of the Figure 3. The existence of the cluster was established both by geometric and energy characteristics. However, the further addition of lithium ions to the channel leads to the dissolution of the cluster, which disappeared already when the number of lithium atoms in the channel was equal to 15.

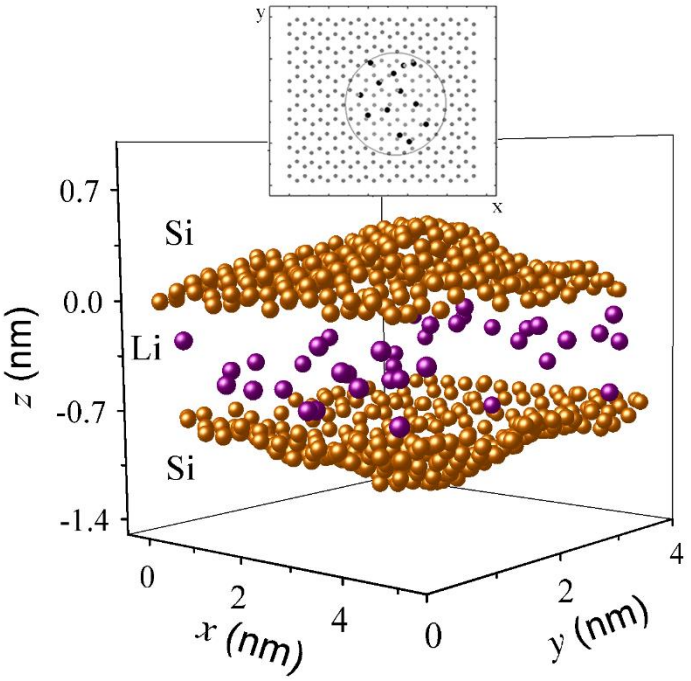

Figure 3 The placement of 38 lithium atoms in the free-standing silicene channel obtained by the time of 0.52 ns. Inset: *xy*-projection of the upper sheet of silicene with the selected area of the flat 13-atomic lithium cluster, related to the time instant 0.15 ns.

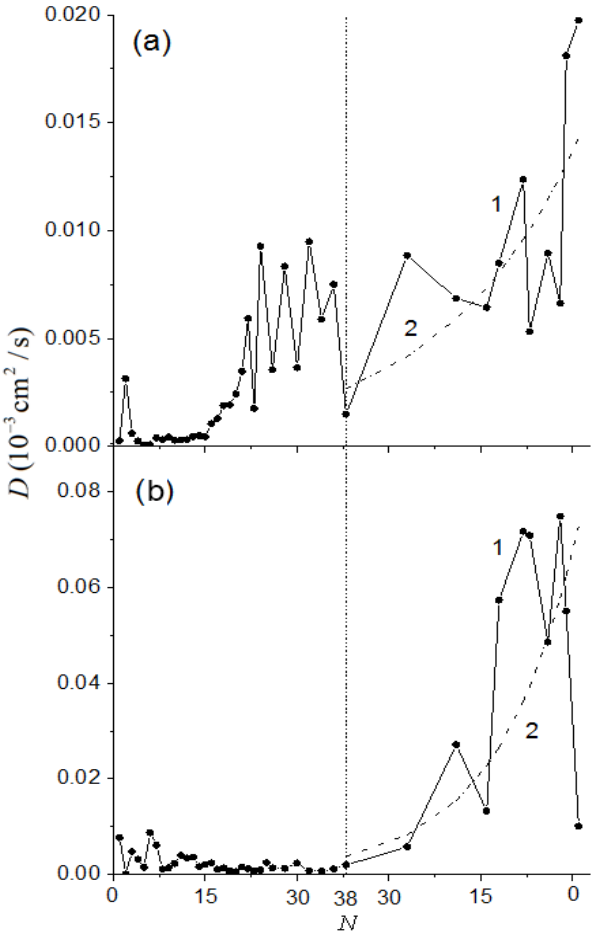

Figure 4 Self-diffusion coefficients *D* of (a) lithium atoms and (b) lithium ions as a function of the number *N* of Li atoms present in the free-standing silicene channel. The left part of the figures (a) and (b) reflects the process of intercalation, and the right part - deintercalation; 1 – dependence *D*(*N*) obtained in the MD model, 2 – exponential approximation of the MD calculation data.

Deintercalation was initiated by the random appearance of two Li^+ ions among the Li atoms in the channel and was maintained by an electric field of the same (as in the case of intercalation) magnitude (10^3 V/m) but in the opposite direction. As a rule, the ions left the channel not singly or in pairs, but taking several Li atoms with them. In [55], the self-diffusion coefficient *D* was determined separately for Li^+ ions and Li atoms. As a result of acceleration by the electric field, the value of *D* for the ions exceeded the corresponding characteristic of the Li atoms by several times (Figure 4). The self-diffusion coefficient for Li atoms after the initial burst exhibits a smooth behavior, turning into strong fluctuations in the region where Li^+ ions were introduced into the channel in pairs. The coefficient *D* for Li^+ ions after initial fluctuations comes to stable values. Initial fluctuations characterize rather a free movement along the channel between collisions of the ion with the walls of the channel or with the atoms that have appeared in the channel. Lithium deintercalation in a free-standing silicene channel proceeds with a sharp increase in the mobility of both ions and atoms. This is due to the manifestation of the Coulomb interaction between ions, the acceleration of ions by an electric field, and the gradual increase in the range of ions due to the release of the channel from ions and atoms. In Figure 4, the rise in the *D* coefficient during deintercalation is reflected by an exponential dependence.

When studying the motion of a lithium ion in a silicene channel with walls containing vacancy defects, a fairly high stability of bivacancies was shown, which retain their shape when ions frequently hit the pore boundaries [56]. By introducing mono- and bivacancies into silicene, it is possible to control the charging/discharging process of the electrode. The size and distribution of defects in silicene affect its mechanical stability. Large polyvacancies, i.e. trivacancies and larger defects, not only weaken the strength of the silicene sheet, but also introduce randomness into the penetration of lithium ions through the silicene [62]. Vacancies in silicene if it is not loaded with lithium create a magnetic moment, and the adsorption of lithium on silicene causes a shift in the Fermi level and charge transfer from Li to the surface [63]. The data obtained can be useful in developing the design of electrodes for more advanced LIBs.

3.2. Computational study of the functioning of the silicene-transition metal anode

3.2.1. Intercalation/deintercalation of Li ions in silicene anode on Ag(111) substrate

When filling with lithium, the silicene channel located on the Ag(111) substrate, the Morse potential was used to describe cross interactions, including interactions between Li atoms (Li^+ ion) and Ag atoms [64–66].

All Morse potentials (Figure 5) used in [43, 61, 67–70] to study intercalation and deintercalation of lithium had

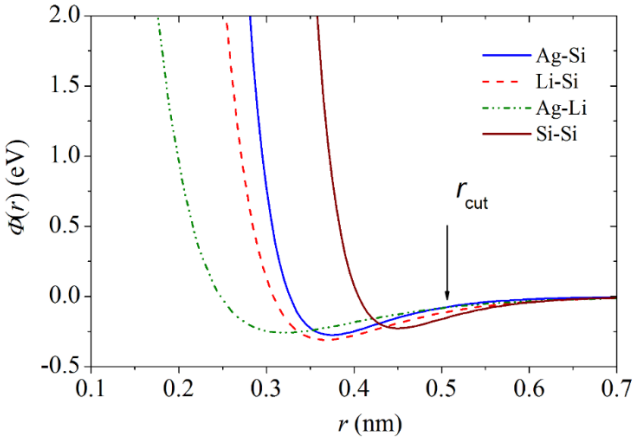

Figure 5 Morse potential describing the interactions: Ag–Si, Li–Si, Li–Ag, and Si–Si between the silicene layers.

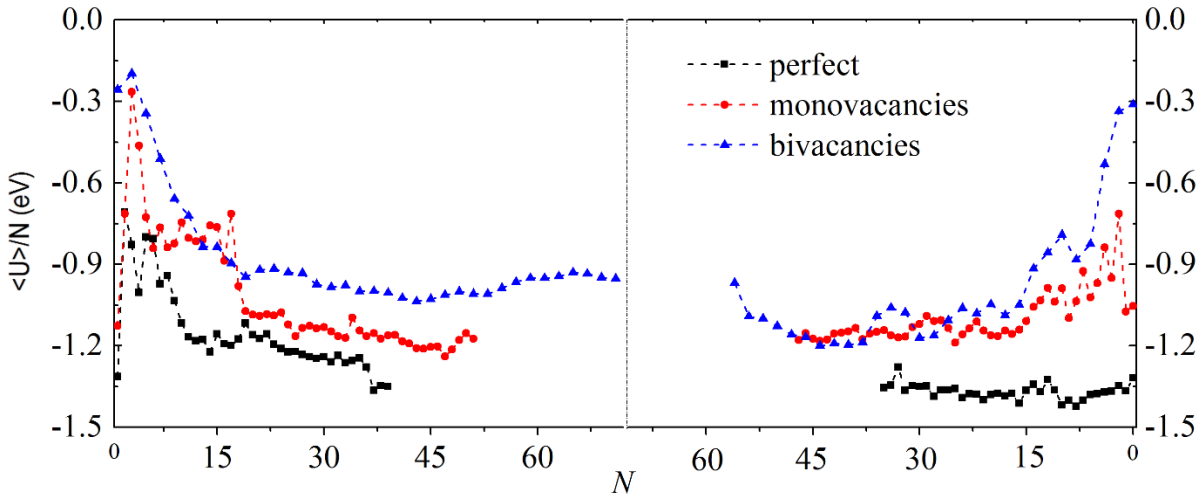

Figure 6 Internal energy of lithium atoms in the process of intercalation (left) and deintercalation (right) in various silicene channels on an Ag(111) substrate. *N* is the number of lithium atoms in the channel.

the same cutoff radius (r_{cut} = 0.5 nm), so that, for example, each silicon atom could interact with silver atoms from no more than two surface layers.

The Morse potentials used to describe the interactions of lithium, silicene with other substrates considered here (Ni, Cu, Al, graphite, silicon carbide) are presented in the *Supplementary Materials*.

Figure 6 shows the behavior of the specific energy $\langle U \rangle$ of lithium during its intercalation (in the figure on the left) and deintercalation (on the right). The abscissa shows the number *N* of the Li atoms in the channel. The graphs reflect the change in $\langle U \rangle$ when the channels are formed by perfect silicene, as well as silicene with mono- and bivacancies. High values of $\langle U \rangle$ at the beginning of channel filling are associated with the free movement of atoms and ions that do not experience deceleration along the channel. A further decrease in $\langle U \rangle$ is defined with the binding of Si atoms to the top and bottom sheets of silicene. Gradually, Li atoms occupy the most advantageous places on the surface of silicene sheets, and the value of $\langle U \rangle$ ceases to be dependent on *N*. The change in $\langle U \rangle$ during deintercalation occurs in the reverse order.

A silicene channel with a gap of 0.75 nm and walls with monovacancies was filled with 51 lithium atoms in 0.51 ns. In order to consider the packing of lithium atoms in a silicene channel located on an Ag(111) substrate, a horizontal plane was drawn through the middle of the channel gap. The view from this plane to the top and bottom sheets of silicene is shown in Figure 7. During the considered period of time, 6 cavities were formed in the top sheet of silicene, and 7 cavities in the bottom sheet, the boundaries of which were formed by more than 6 Si atoms. Moreover, the two largest cavities are on the bottom sheet. Despite the fact that the upper and lower

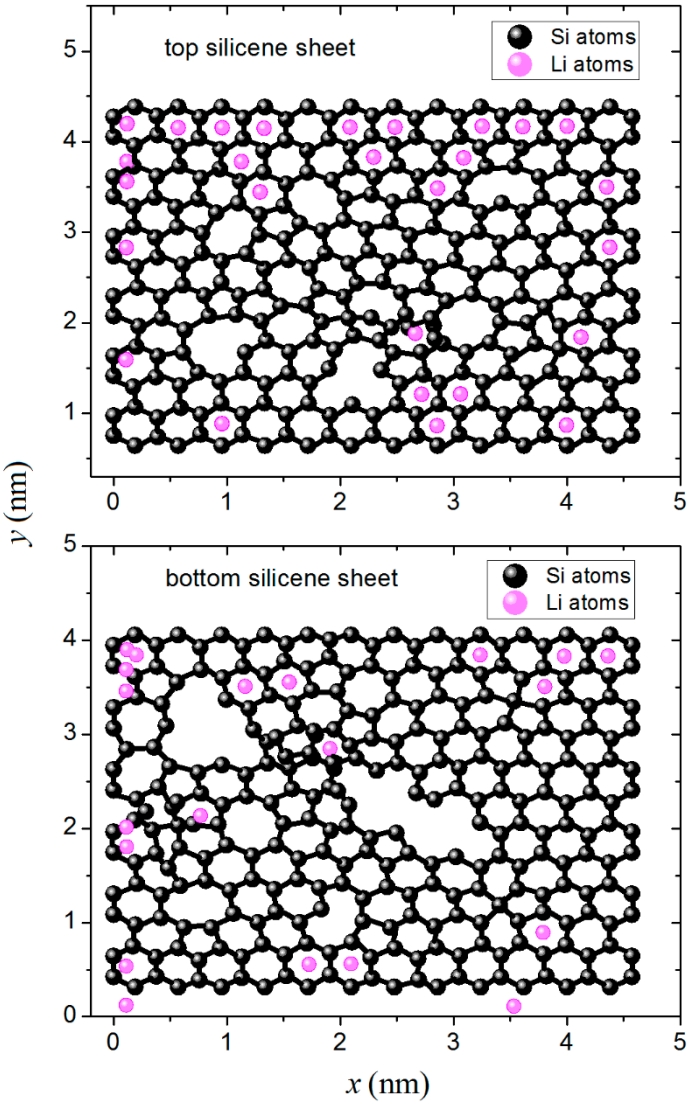

Figure 7 *Xy*-projections of the upper and lower sheets of silicene with monovacancies on the Ag (111) substrate, at the time of complete lithiation (51 lithium atom was adsorbed on the silicene surface).

parts of the channel have approximately the same volumes, they are adjacent to a different number of Li atoms: 27 Li atoms to the top sheet and 20 Li atoms to the bottom sheet; 4 Si atoms (not shown in Figure) fell on the virtual horizontal plane. Most of the Si atoms adjacent to the top sheet and half of the Si atoms belonging to the bottom sheet are located above the centers of the hexagonal Si rings.

Figure 8 shows the change in the self-diffusion coefficient of Li atoms upon intercalation and deintercalation of lithium into silicene channels formed by perfect silicene, as well as silicene containing mono- and bivacancies. When the channel was formed by perfect sheets, it was possible to fill it with only 39 Li atoms. In the case of the presence of monovacancies in silicene sheets, 51 Li atoms were placed in the channel, and in the presence of bivacancies, the number of lithium atoms that entered the channel increased to 71. The mobility of the atoms in the channel with bivacancies was significantly higher than in other cases. This is due to the fact that, in the presence of divacancies, Li^+ ions were launched into the channel in pairs rather than individually, as in the previous cases. Due to the Coulomb interaction between ions, the number of collisions between atoms and their frequency has increased. The fluctuations of the coefficient *D*, observed during the filling of the channel with ions, also increased.

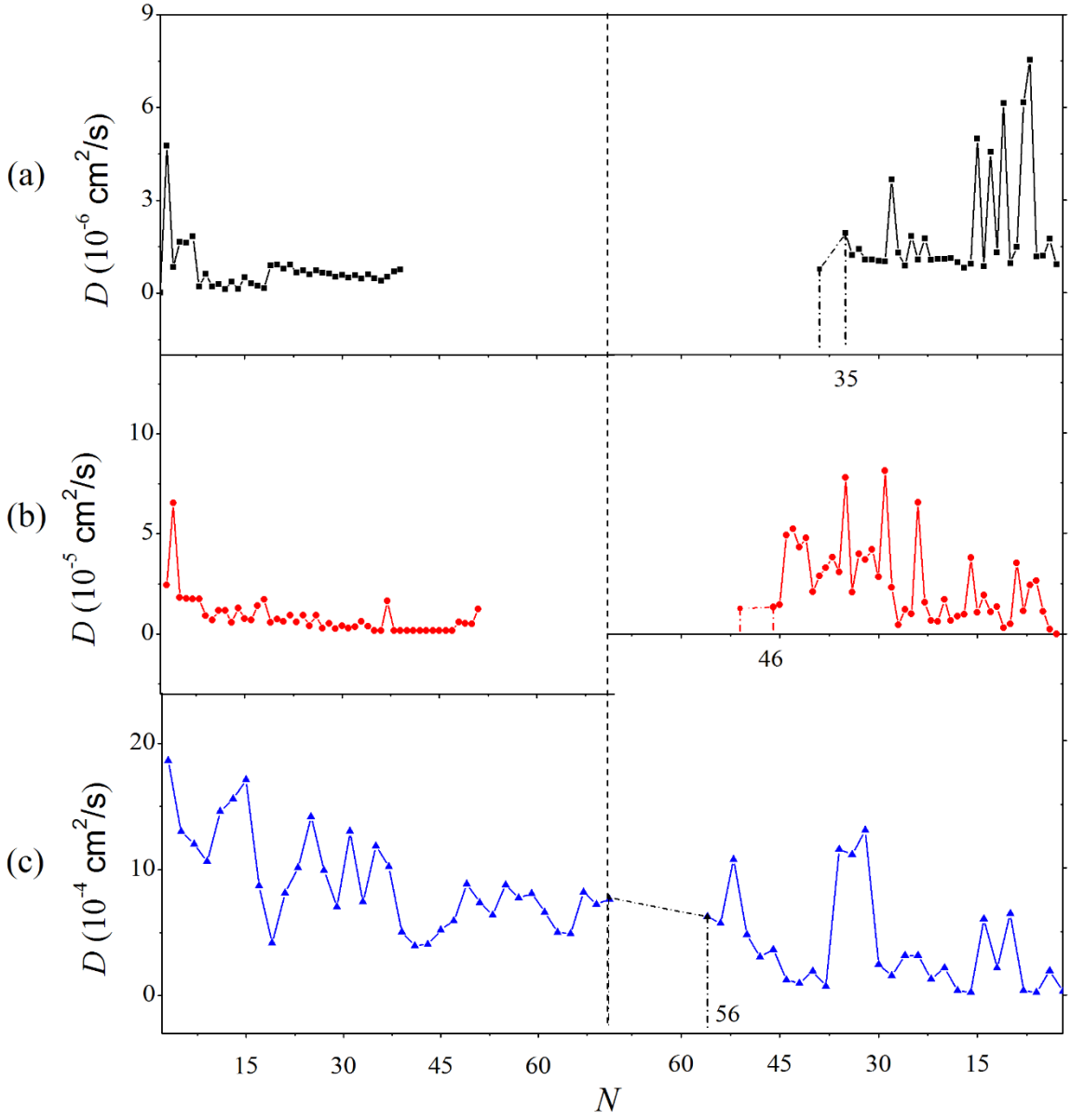

Figure 8 The coefficient of self-diffusion of lithium atoms in the process of intercalation (left) and deintercalation (right) in silicene channels on Ag(111) substrate; characteristic of the channel walls: (a) perfect, (b) with monovacancies, (c) with bivacancies. Removal of the lithium atoms that are outside the channel before the start of deintercalation is marked in the figure by dashed lines and dot-dash lines.

During deintercalation, ions left the channel in the reverse order with respect to their entry into it. The behavior of *D* during deintercalation looks largely chaotic due to the arbitrary placement of lithium ions assigned to leave the channel. The self-diffusion coefficient of lithium during its deintercalation has much larger fluctuations than during intercalation. This is due to more or less similar conditions for the onset of intercalation of Li^+ ions in the system and very different conditions for the deintercalation of ions, which can occupy very different places in the silicene channel and have different local channel shapes and different lithium environments.

Since the lithium atoms in the channel interact both with each other and with the channel walls, it makes sense to consider two types of statistical distribution obtained by constructing Voronoi polyhedra. In the first case, the neighbors of Li atoms can be Li atoms, and in the second case, the neighbors of these atoms can include both Li atoms and Si atoms. Both types of distributions are shown in Figure 9 in the case where the silicene channel is formed by sheets of perfect silicene. When the channels are formed from sheets of defective silicene, the distinguishing features between the distributions of the two types do not change. A large number of 4–6-faced polyhedra (about 44 %) in the distribution of polyhedra in terms of the number of faces with a maximum at $n = 5$ is observed when the n distribution is constructed on the basis of considering only Li atoms. When Si atoms also attach to neighboring atoms, the maximum of the n distribution is shifted by $n = 9$. Depending on which neighbors are taken into consideration, the distribution of faces by the number of sides (m spectrum) also changes. Faces with $m = 4$ (31 %) dominate in the m-distribution based on the analysis of polyhedra of the first type. The location of the maximum of the m distribution does not change when polyhedra of the second type are used for its construction. However, the proportion of quadrangular faces in this case decreased to 25 %. The shape of the angular distribution changes very little when Si atoms are included in the number of geometric neighbors.

The performed calculations showed that vacancy-type defects in silicene sheets placed on a silver substrate are not sufficiently stable. This creates a problem in using silicene on an Ag(111) substrate as an anode material.

The use of silicene with vacancy defects for this purpose is expedient, because defects increase the adsorption capacity of the flat channel and, consequently, lead to an increase in the charging capacity of the silicene anode. Another disadvantage of this anode design is the relatively high cost of the substrate material. In addition, Ag is a sufficiently heavy metal that its use in LIBs will reduce the gravimetric energy density of the battery.

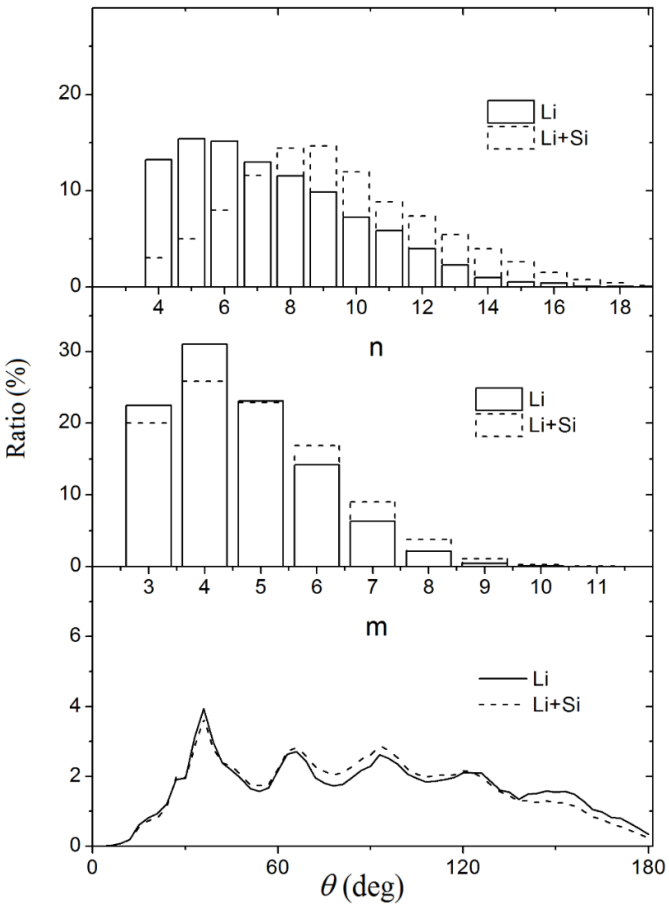

Figure 9 Distribution of VP with respect to the number of faces (n), distribution of faces by the number of sides (m) and distribution of angles (ϑ) formed by the nearest geometric neighbors. VP are constructed for Li atoms in the case when they completely fill a flat silicene channel formed by perfect silicene sheets on Ag (111) substrate. The neighbors were formed either by Li atoms or by together Li and Si atoms forming channel walls.

3.2.2. Silicene on Ni (111) substrate as anode material of lithium-ion battery

High electrical conductivity, low cost, and good adhesion to Si stimulated the use of nickel as an inactive material in the design of the LIB anode [71]. Silicon has a high solubility in nickel, so good adhesion of Si to Ni substrate was observed. At the same time, the solubility of Ni in bulk silicon is extremely low. Bulk silicon has a low electrical conductivity, which significantly impairs battery cycling. When Si is deposited on a Ni(111) substrate at room temperature, a disordered 2D and/or 3D intermetallic compound is formed [72]. Si atoms are in strong interaction with Ni atoms and are embedded in the uppermost surface layer of nickel. Although the method for obtaining a continuous extended Si film on a nickel substrate has not yet been developed, it is of interest to study the behavior of silicene on a Ni(111) substrate during intercalation and deintercalation of lithium. The special

structure of silicene obtained by mixed sp^2 and sp^3 hybridization allows us to hope for a stable heterostructure in the form of silicene on a nickel substrate.

Molecular dynamics studies of lithium intercalation and deintercalation in a silicene channel on a nickel substrate are the subject of [73–77]. The filling of the silicene channel located on the Ni(111) substrate with lithium occurs upon a strong vertical deformation of the silicene sheets. The resulting distortion of the channel shape is accompanied by a reduction in its volume, which in the case of perfect silicene reaches 22 %. However, the presence of vacancy defects in the silicene sheets weakens vertical deformations until the defects become large. Thus, in the presence of hexavacancies, the decrease in the channel volume after its filling with lithium was ~25 %. A change in the shape of the silicene channel affects the distribution of lithium atoms in it. Figure 10 shows the number density profiles for packing lithium in a channel formed by silicene sheets with trivacancies. The entrance to the channel and the level of the lower sheet of silicene are represented by the values $x = 0$ and $z = 0$, respectively.

The shape of the horizontal density profile indicates the uneven filling of the channel with lithium, with the highest filling intensity falling on the intervals $1 < x < 2$ and $3.0 < x < 3.6$.

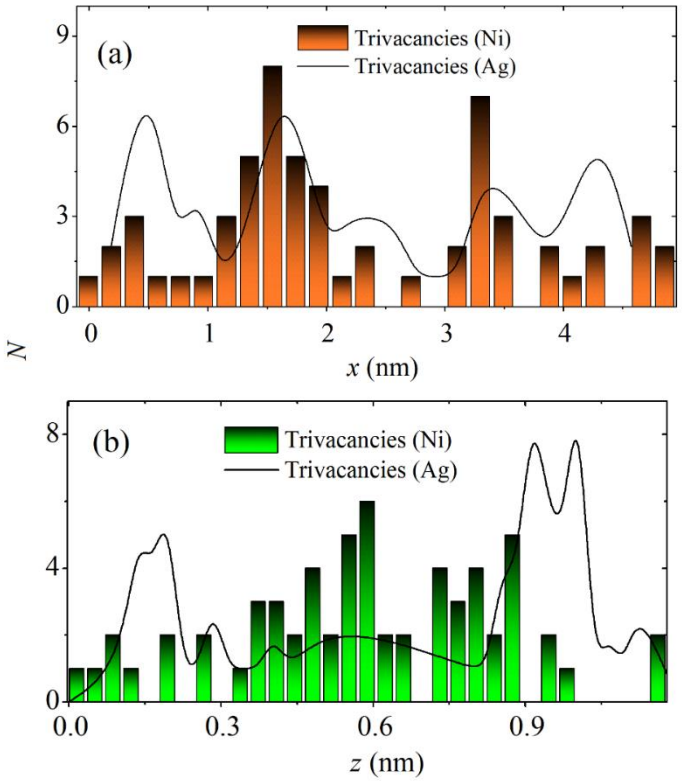

Figure 10 (a) Horizontal (longitudinal) and (b) vertical profiles of lithium density in a silicene channel with trivacancies on Ni(111) and Ag(111) substrates.

In the presence of the Ni(111) substrate, the morphology of the filling of the channel with lithium changes with respect to the morphology observed in the channel on the Ag(111) substrate. The uneven filling of the channel on the Ag(111) substrate was expressed in a higher population in the first half of the channel length (57.5 %) and in a lower population in the second half (42.5 %). The study of the occupancy of the channel along its height shows that in the channel on the Ni(111) substrate, the middle part of the intersheet space is mainly filled, while the walls contain few Li atoms. A different picture is observed for the channel on the Ag(111) substrate, where the content of Li atoms in space at the level of the middle of the channel height is not high, mainly Li atoms tend to be located near the surface of silicene sheets.

After filling the channel with lithium, the shape of vacancy defects in the channel walls on the Ni(11) substrate changed. If we draw a plane through the middle of the channel height parallel to the silicene sheets, then the view of the channel walls containing trivacancies from the side of this imaginary plane at the time of 0.6 ns will be determined by the image shown in Figure 11.

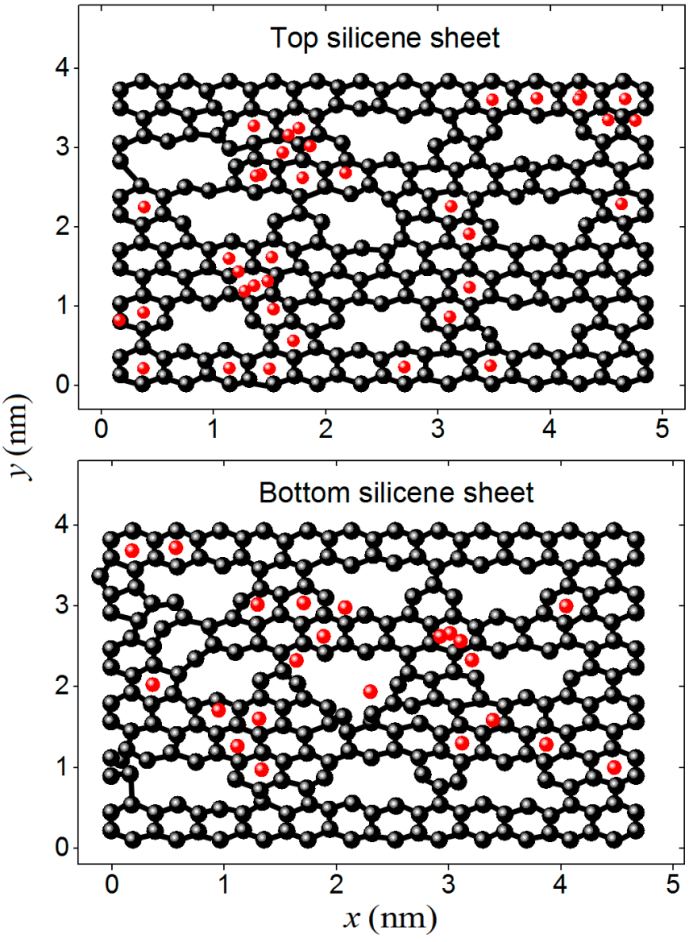

Figure 11 *Xy*-projections of the upper and lower sheets of silicene with trivacancies on the Ni(111) substrate, at the time of complete lithiation (60 lithium atom was adsorbed on the silicene surface). Si atoms form a network.

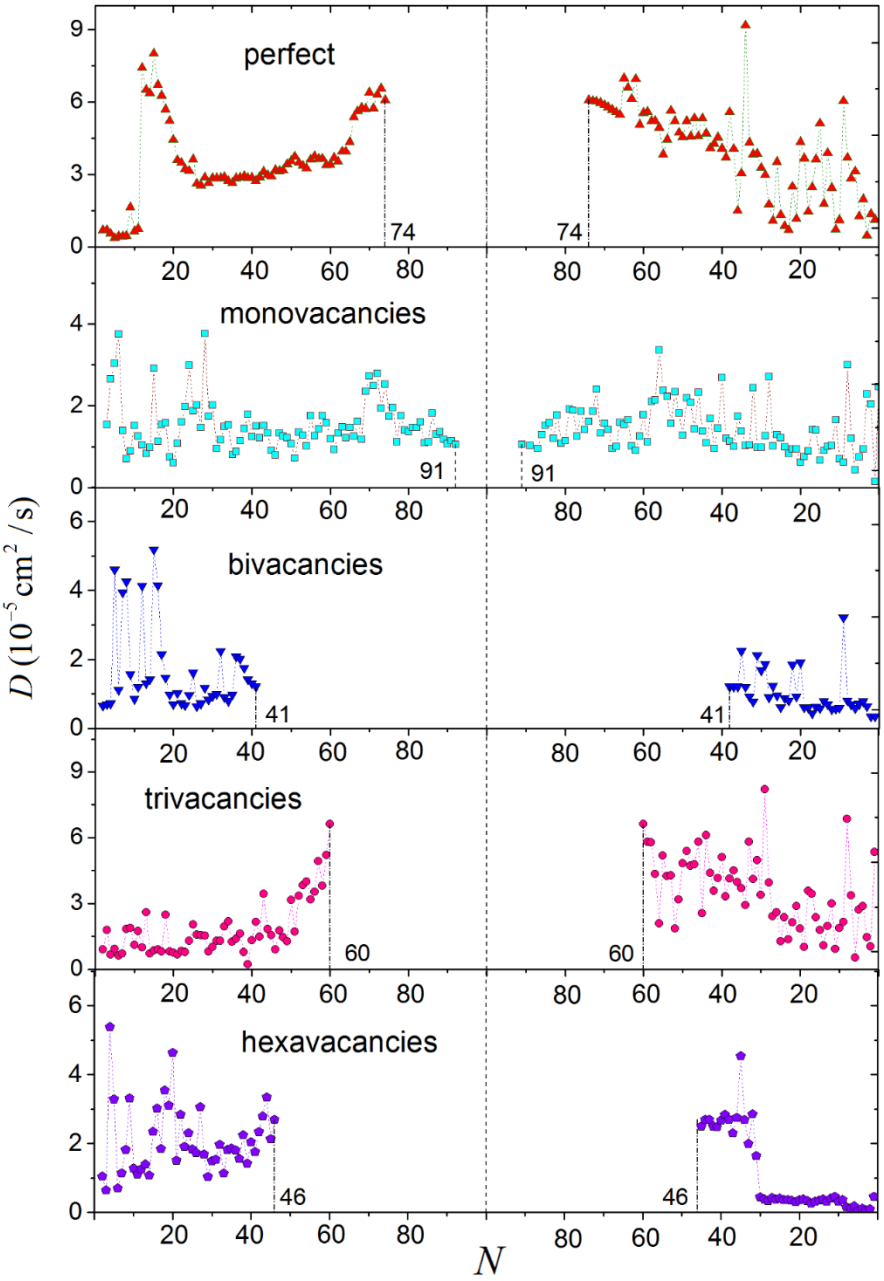

Figure 12 The coefficient of self-diffusion of lithium atoms in the process of intercalation (left) and deintercalation (right) in different silicene channels on a Ni(111) substrate. The maximum achievable number of lithium atoms in the channel is marked with a dash-dotted line.

As can be seen from the figure, the shape of defects is better preserved in the top sheet of silicene. It can be found that after dividing the channel volume by a virtual horizontal plane, the filling of the upper and lower halves of the channel with lithium is not equivalent. The top half contains 37 Li atoms, while the bottom half contains only 23 Li atoms. Regardless of which sheet the Li atoms belong to, most of them are located above the centers of the hexagonal rings formed by the Si atoms. The close proximity of the nickel substrate does not favor the deposition of lithium atoms on the wall of the silicene channel.

The change in the self-diffusion coefficient of Li atoms in the channel on the Ni(111) substrate during intercalation and deintercalation is shown in Figure 12. The highest filling of the silicene channel (91 Li atoms) was achieved when the channel walls contained monovacancies. At the same time, in the presence of bivacancies in the channel walls, its filling turned out to be the lowest (41 Li atoms). The strongest fluctuations in the value of *D* are observed at the initial stage of intercalation, when the number of Li atoms introduced into the channel does not exceed 28. The final stage of intercalation, as a rule, occurs with a smoother behavior of the coefficient *D*.

An exception is the case when the channel walls contain trivacancies. This is largely due to the change in the shape of the channel during intercalation. Significant fluctuations in the coefficient *D* also occur during lithium deintercalation, but when not many lithium atoms were intercalated into the channel (cases with bi- and hexavacancies), deintercalation proceeds more smoothly.

The location of a large number of Li atoms intercalated into a channel placed on a Ni(111) substrate leads to the appearance of a number of peaks in the angular distribution of the nearest geometric neighbors (Figure 13). These peaks are at 30 °, 60 °, 90 °, 120 ° and 150 °. A comparison of ϑ distributions for lithium packings in channels on Ni(111) and Ar(111) substrates shows that the peaks in the ϑ distribution on a metal substrate are more intense, which is due to a larger number of Li atoms located above Si hexagonal rings. Note that when Si atoms are also included in the number of nearest neighbors, and trivacancies or hexavacancies are present in the walls of the silicene channel, a peak appears in the ϑ distribution at ϑ = 0 ° of not low intensity. This means that quite often among the triplets of atoms participating in the construction of VP there are cases when they (atoms) all lie on the same straight line. Moreover, in most cases, in the composition of such triplets of atoms, there is a Si atom, because the corresponding ϑ distributions constructed exclusively for the Li subsystem do not have peaks of such intensity at ϑ = 0 °.

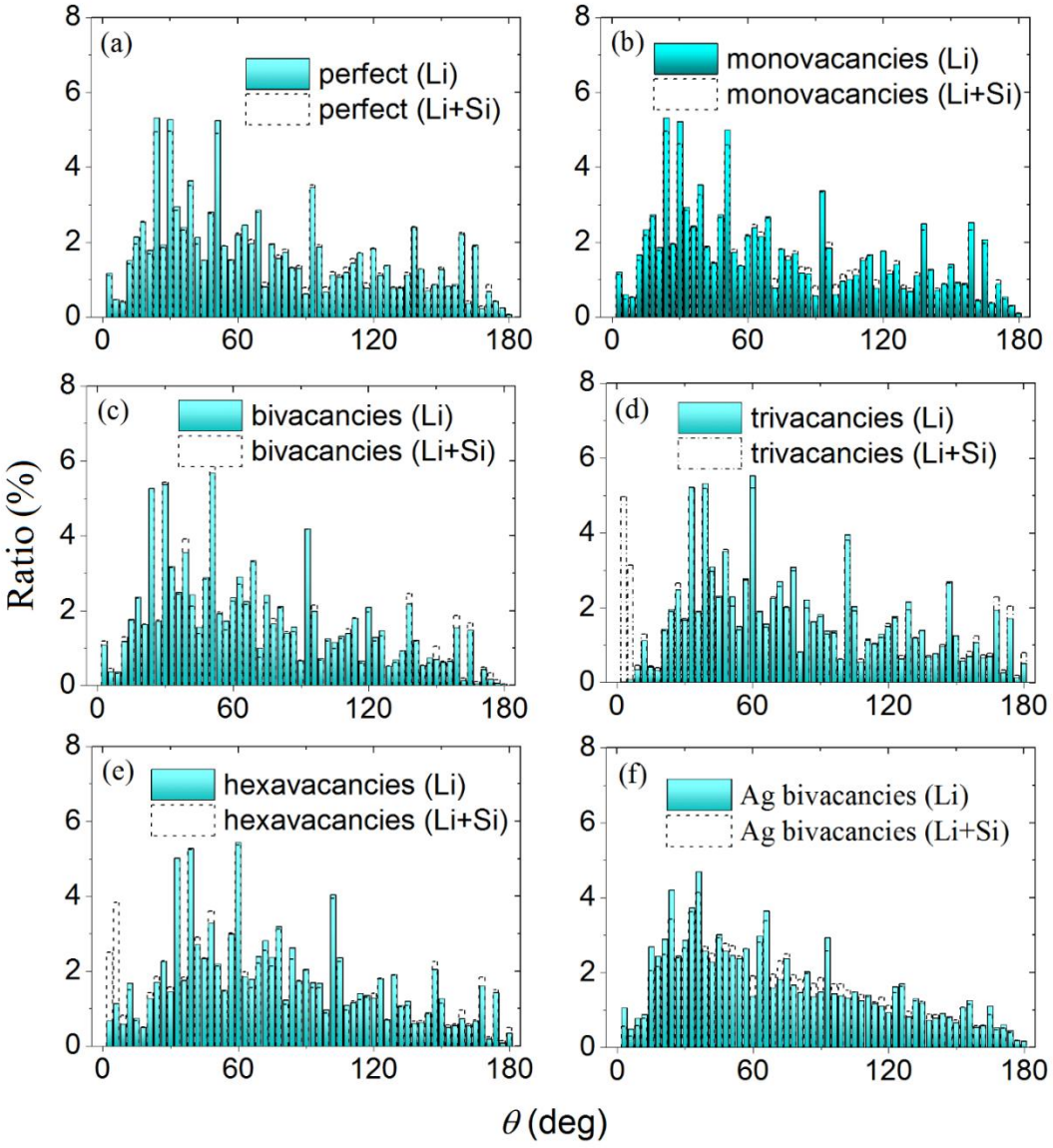

Figure 13 The angular distribution of the nearest neighbors for lithium atoms after instant when the silicene channel is completely filled: (a) – (e) on a Ni(111) substrate, (f) on an Ag(111) substrate. Solid (colored) histograms are obtained when only Li atoms represent neighbors; dotted histograms correspond to the case when neighbors are selected from both Li atoms and Si atoms. The types of defects in silicene and the neighbors under consideration (in parentheses) are indicated in the captions in the margins of figures (a) – (f).

In the case of perfect walls of a silicene channel and for a channel with walls having monovacancies, the distribution of VP over the number of faces has an approximately dome-like shape, which disappears with the enlargement of vacancy defects in the channel walls (Figure 14). This applies not only to the *n* distribution, which belongs to the purely lithium subsystem, but also to the addition of the nearest geometric neighbors by Si atoms. There is a significant difference in the *n* spectra obtained for silicene channels containing bivacancies located on Ni(111) and Ag(111) substrates. This means that nickel and silver substrates have different effects on the formation of Li atom packing in the channel.

The stresses acting in the direction normal to the surface of the silicene sheets turn out to be the strongest when lithium atoms are introduced into the silicene channel. Figure 15 shows the stresses averaged over both silicene sheets, which were obtained at the final stage of filling the channel on a Ni(111) substrate, with lithium (at $N_{Li} > 30$). As can be seen from the figure, the most significant normal stresses arise in the walls of a perfect silicene channel, as well as in the channel walls containing mono- and trivacancies. Normal stresses of the same order were observed when lithium filled a silicene channel, which had monovacancies in the walls, when the channel was located on an Ag(111) substrate.

Molecular dynamics modeling has shown that, in contrast to the Ag(111) substrate, the Ni(111) substrate maintains the shape of defects in the walls of the silicene channel much better when it is filled with lithium.

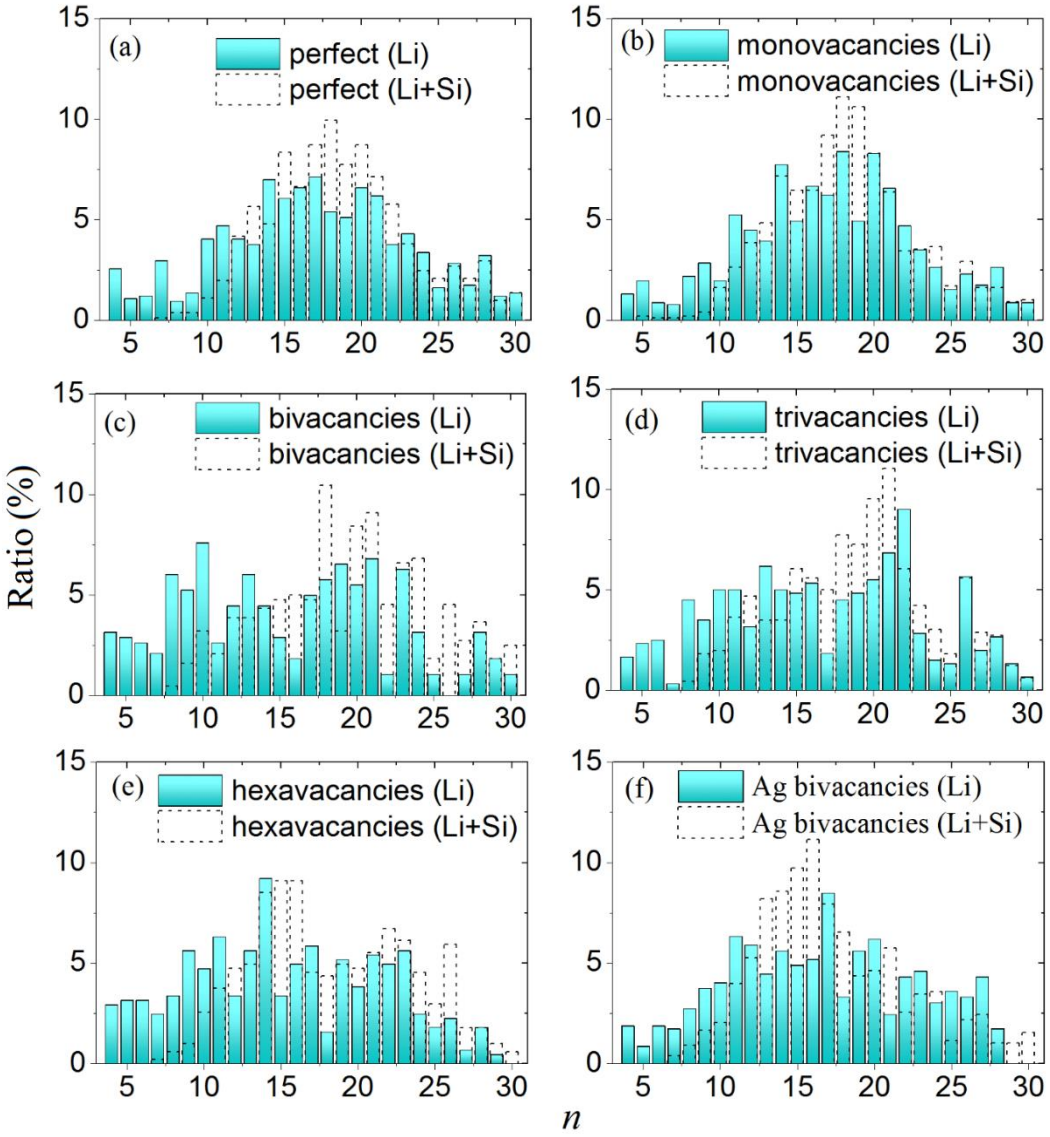

Figure 14 The distribution of Voronoi polyhedra with respect to the number of faces (n). VPs are built for lithium atoms after the complete filling of a silicene channel, which is located: (a) – (e) on a Ni(111) substrate, (f) on an Ag(111) substrate. Solid (colored) histograms present the case when only Li atoms represent neighbors; dotted histograms give an idea of the local packing of atoms when neighbors are selected from both Li atoms and Si atoms. The types of defects in silicene and considered neighbors (in parentheses) are indicated in the captions in the margins of figures (a) – (f).

Due to the higher adhesion between nickel and silicene (compared to the adhesion between silicene and silver), the self-diffusion coefficient of lithium atoms responds to a change in the size of defects in silicene to a lesser extent than in the case of using an Ag(111) substrate. In addition, on the Ni(111) substrate, a larger number of lithium atoms deposited on the channel walls are located above the centers of hexagonal Si rings than in the case of using the Ag(111) substrate. All these effects inherent in the use of Ni(111) substrates contribute to a higher level (more than 10 % on average) of filling the channel with lithium during intercalation and free passage of the deintercalation process. Calculations show that silicene on a nickel substrate is suitable for use as an anode material. However, for the real use of such a heterostructure, it is necessary to create a technology for obtaining thin silicon films on nickel. The maximum local stress on the walls of a lithium-filled silicene channel does not exceed 18 % of the maximum tensile stress determined for silicene [78].

3.2.3. Applicability of silicene on Cu(111) substrate as anode material of lithium-ion battery

Although silicene on a copper substrate has not yet been obtained, copper films on various silicon substrates have been repeatedly studied [79]. Moreover, the copper film on Si acquires a high hardness (2.5 GPa) [80]. The difficulty in obtaining a homogeneous thin film of copper is that Cu atoms easily diffuse into silicon.

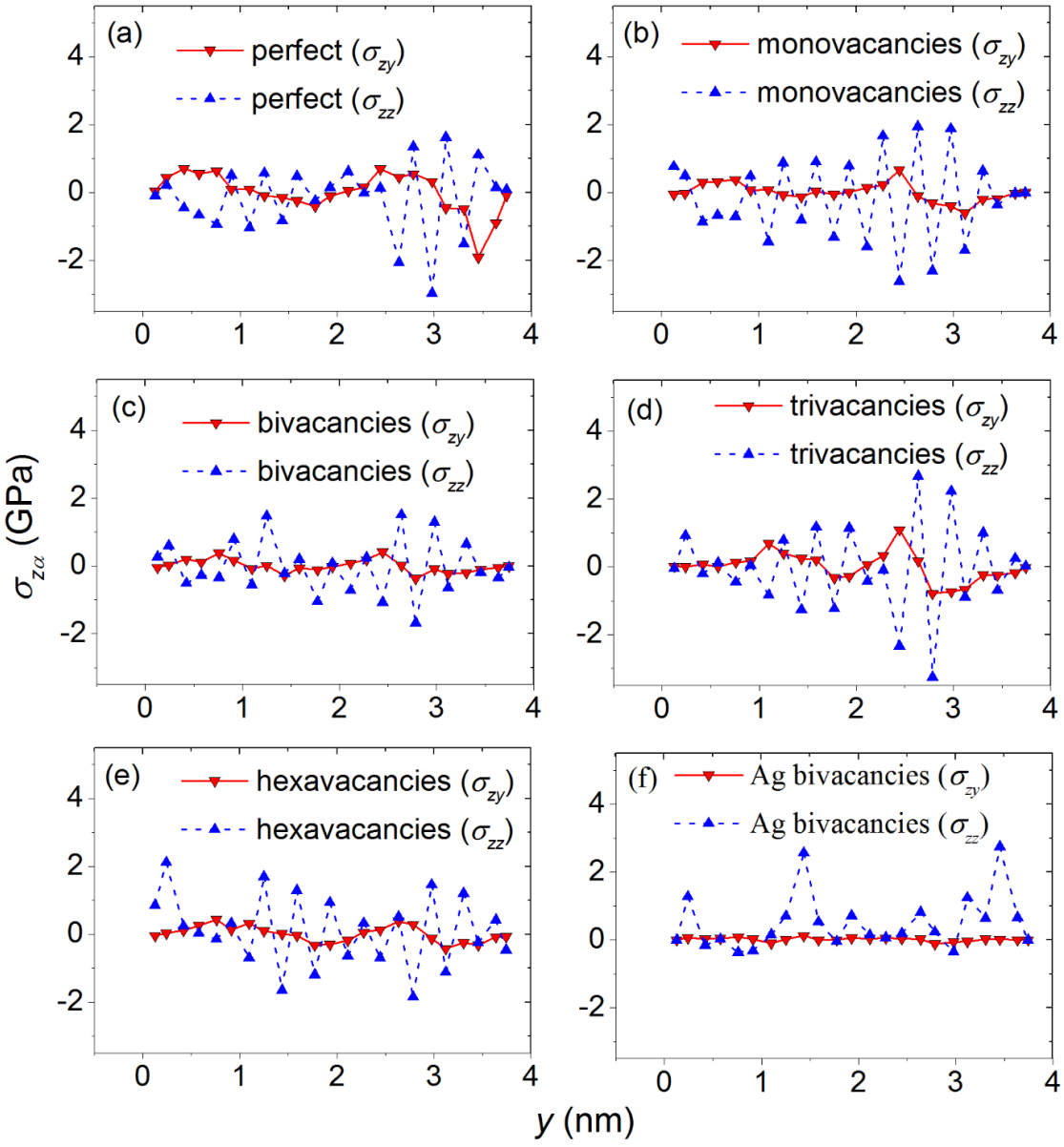

Figure 15 The distribution of the average σ_{zx} and σ_{zz} stresses in the sheets of silicene along the *oy* (armchair) direction when lithium is intercalated in a silicene channel located on a Ni(111) substrate. Elementary platforms are elongated along the axis *ox*. The types of defects in silicene and the stresses in question (in parentheses) are indicated in the captions in the margins of figures (a) – (f).

Films of polycrystalline tantalum and amorphous tantalum nitride can serve as a barrier for diffusion of copper atoms [81]. Such barriers are highly stable, because no Ta–Cu compound is formed.

Currently available methods will not be able to produce silicene in sufficient size and quality. The production of copper silicide $Cu_{(3+x)}Si$ presumably can be considered as one of the ways of industrial production of silicene. The $Cu_{(3+x)}Si$ structure contains ready-made monatomic silicon layers with a silicene-like arrangement of Si atoms. Copper silicide can be produced by low pressure chemical vapor deposition (CVD) or by magnetron sputtering on Si or Cu substrate. Then, by selective chemical etching of copper, free-standing silicene can be obtained and transferred to the desired substrate. The copper silicide film can be obtained over a large area. Thus, the problem of obtaining silicene on a large area surface can be solved. Methods for separating silicene from a native substrate and transferring it to an arbitrary target substrate are being developed [82]. In [83, 84], a molecular-dynamic study of the behavior of two-layer silicene on a Cu(111) substrate when it is used as an anode material was performed. A silicene channel with walls containing hexavacancies located on a copper substrate experienced significant structural rearrangements during lithium intercalation and began to break down. It was assumed that such a material is not suitable for an anode construction [83], and this variety of research is not considered further.

The horizontal and vertical density profiles of lithium in silicene channels with an initial gap of 0.75 nm at the moment of its complete filling with lithium are shown in Figure 16. In the case of a channel with perfect silicene walls, as it is filled with lithium, the permeability deteriorates, as a result of which lithium is concentrated in the initial part of the channel. However, the presence of vacancy defects in the channel walls unloads its initial part when filled with lithium, and a higher value of lithium density shifts to the middle part of the channel. In the presence of bivacancies in silicene, a high density of lithium is also formed at the outlet of the channel. Filling a channel with perfect walls leads to the formation of a gap of 0.15 nm in the middle part of the vertical profile. This gap separates the channel into upper and lower parts. Moreover, about 58 % of all Li atoms located in the channel are located in the lower part of the channel. The gap disappears in the presence of vacancy defects in silicene, and the lithium density in the middle part of the channel increases. When the channel walls contain bivacancies, the number of Li atoms in the previously determined lower part of the channel is reduced to 53 %.

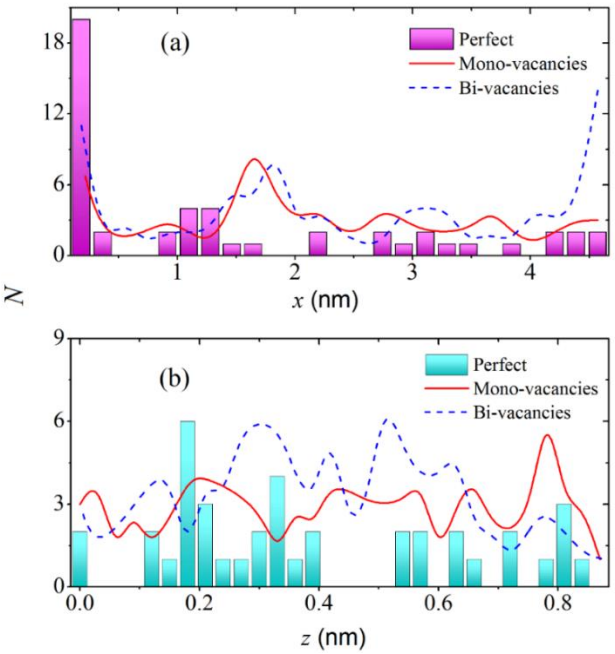

Figure 16 Horizontal (longitudinal) and vertical profiles of lithium density in silicene channels on the Cu (111) substrates.

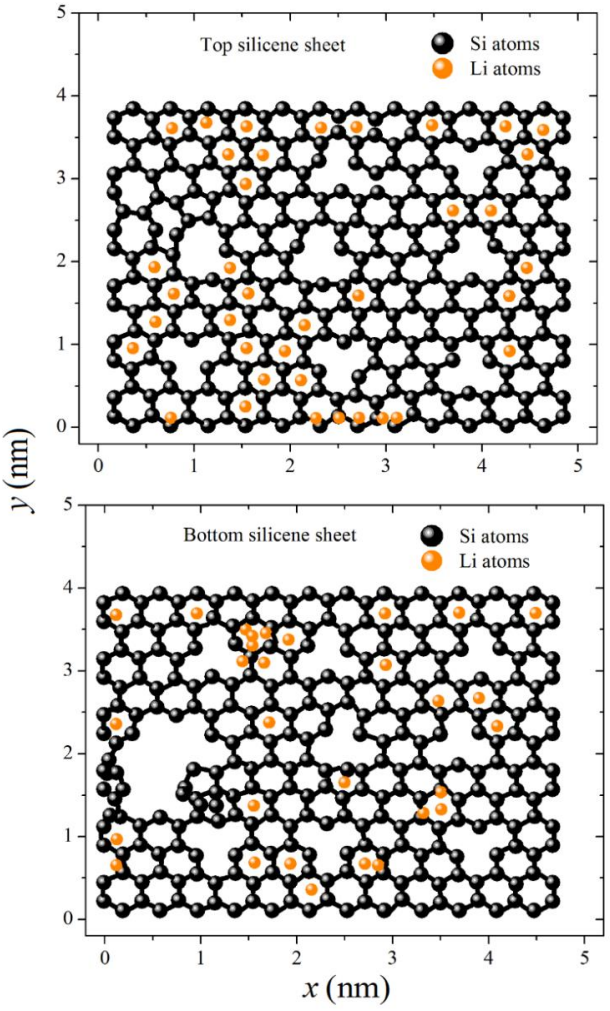

Figure 17 The *xy* projections of the upper and lower sheets of silicene with mono-vacancies on the Cu(111) substrate at the instant of complete lithiation (67 lithium atoms are in the channel).

The configurations of the monovacancy silicene sheets after completion of filling the channel with lithium, together with their associated Li atoms, are shown in Figure 17. The view of the bottom sheet from the side of a virtual horizontal plane drawn through the middle of the channel height reflects the strongly altered structure of silicene. As a result of the union of two monovacancies of the bottom sheet, a large hole was formed due to the destructive effect of the copper substrate on the silicene. The remaining vacancies in the bottom and top sheets have not changed much from their original form. It can be seen from the figure that 37 Li atoms belong to the top sheet of silicene, while only 30 Li atoms belong to the bottom sheet.

At the initial stage of intercalation, high self-diffusion coefficients of Li atoms are observed in all types of channels considered (Figure 18). At this stage, in the presence of a significant freedom to move, a large value of the specific impulse is transferred from Li^+ ions to Li atoms, which leads to an increase in the value of *D*. When the number of Li atoms in the channel becomes more than 20, the relief of the channel walls begins to play a decisive role in the movement of Li atoms. In this case, in the presence of monovacancies in the channel walls, the value of *D* decreases, while in the case of the presence of bivacancies in the walls, *D* increases. During deintercalation, ions left the channel in the reverse order of their entry into the channel. In this case, in channels with perfect walls and in the presence of monovacancies in the walls, fluctuations in the value of *D*, as a rule, exceed the corresponding fluctuations observed during lithium intercalation. However, the relationship between fluctuations is reversed when there are bi- and trivacancies in the walls. Due to the influence of the relief of the channel walls, the downward trend in *D* begins to manifest itself first of all in the presence of bivacancies in silicene. Here, fluctuations of *D* do not decrease until the end of deintercalation.

The angular distributions of the nearest geometric neighbors obtained during the first half of lithium deintercalation in the channel located on the Cu(111) substrate are shown in Figure 19. Sharp peaks in the angular distributions characterize a certain regularity in the packing of Li atoms, due to their placement above the centers of hexagonal Si rings. Five sharp peaks in the range 0 °–180 ° with a multiplicity of 30 ° are traced in the ϑ distribution in the case of a channel with perfect silicene walls. The location of sharp peaks and their number change when there are vacancy defects in the channel walls. So, in the presence of trivacancies in silicene, only two sharp bursts remain in the ϑ spectrum. Thus, during the period of deintercalation, some of the Li atoms continue to remain above the centers of the hexagonal Si cells.

However, the larger the size of defects in silicene sheets, the weaker this effect is. When Si atoms are included in the number of nearest geometric neighbors, this feature of the regular packing of atoms becomes stronger.

The topological characteristics obtained on the basis of the construction of ordinary Voronoi polyhedra provide too detailed the structure information, that contains thermal fluctuations of atoms. Such characteristics are difficult to analyze. However, to a large extent, thermal fluctuations can be excluded from consideration by passing to the construction of simplified polyhedra [85]. We will denote the simplified polyhedra constructed for the autonomous packing of Li atoms in the channel as SVP, and similar polyhedra reflecting the structure of the extended packing of Li atoms through the SCP (simplified combined polyhedra). The extension implies the inclusion of Si atoms belonging to the channel walls in the number of nearest neighbors.

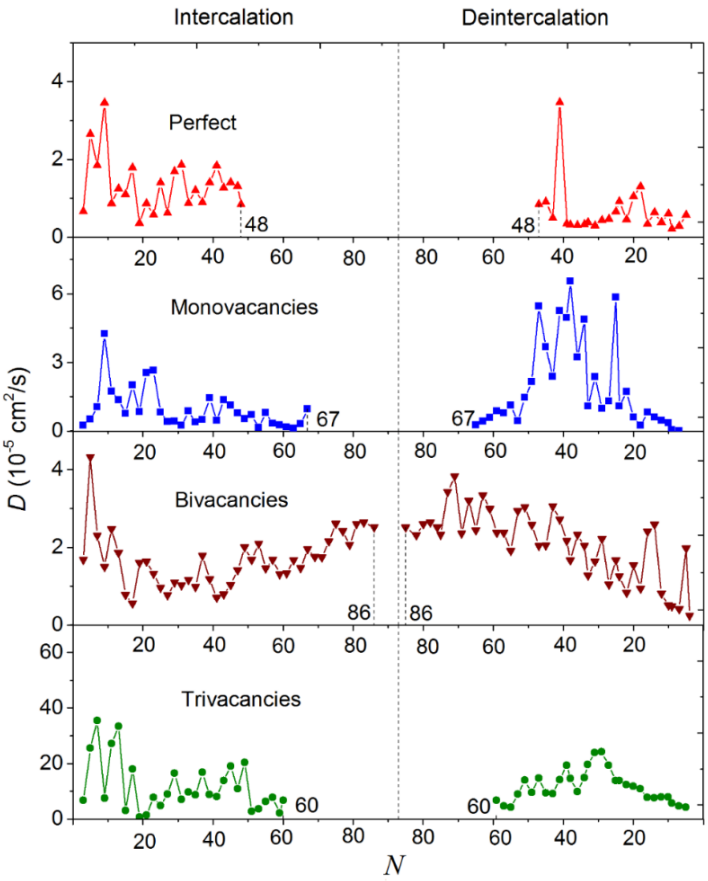

Figure 18 The coefficient of self-diffusion of lithium atoms in the process of intercalation (left) and deintercalation (right) in silicene channels with perfect walls and silicene sheets having mono-, bi-, and trivacancies; the channels are located on the Cu(111) substrate.

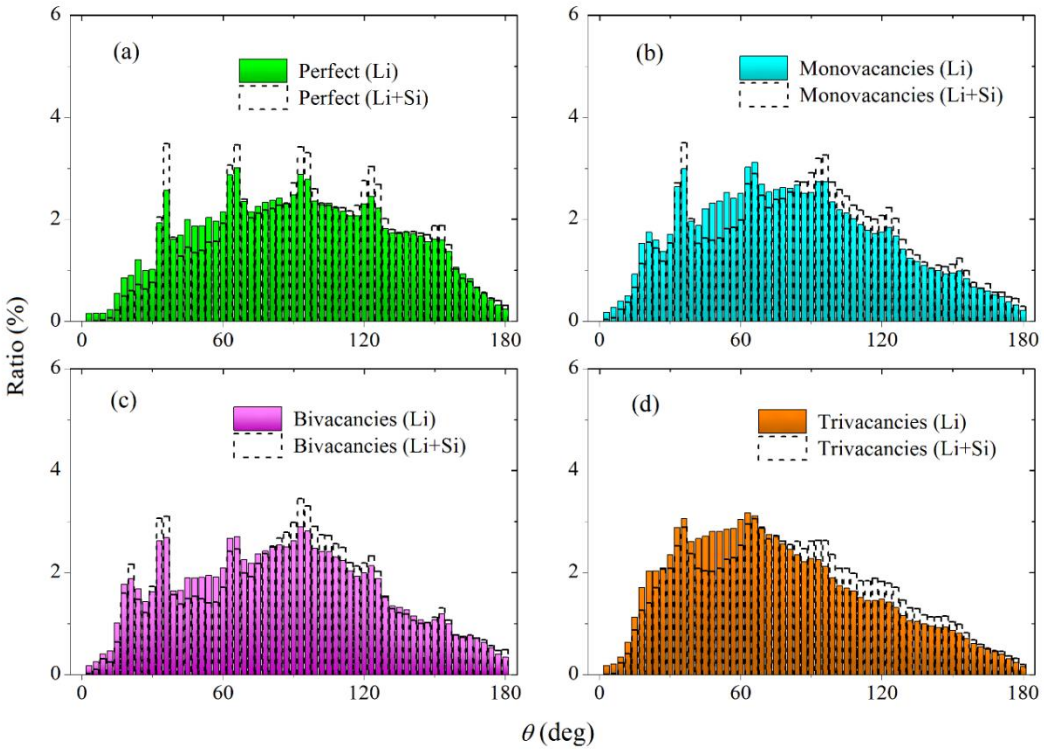

Figure 19 The angular distribution of the nearest neighbors for lithium atoms in the period of deintercalation, when 30 Li atoms are left in the channel: (a) – (d) on a Cu(111) substrate. Solid (colored) histograms are obtained when only Li atoms represent neighbors; dotted histograms correspond to the case when neighbors are selected from both Li atoms and Si atoms. The types of defects in silicene and the neighbors under consideration (in parentheses) are indicated in the captions in the margins of figures (a) – (d).

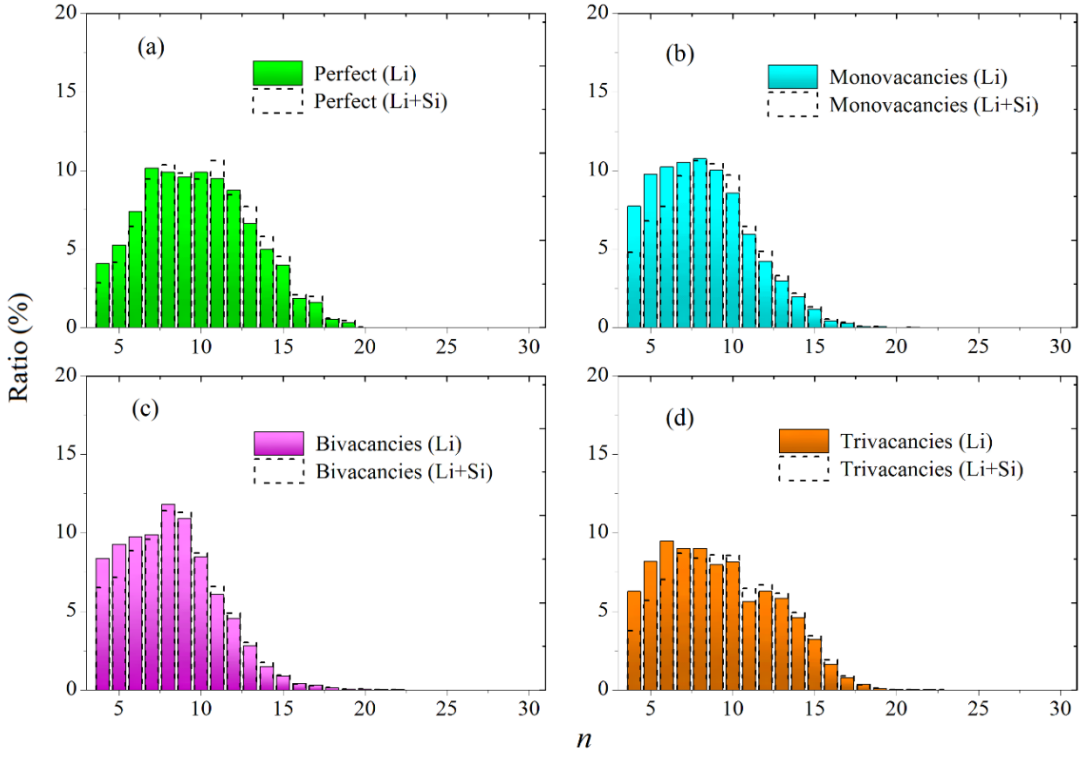

Figure 20 The distribution of simplified polyhedra with respect to the number of faces (n). Simplified polyhedra are built for lithium atoms after the complete filling of a silicene channel, which is located: (a) – (d) on a Cu(111) substrate. Solid (colored) histograms present the case when only Li atoms represent neighbors; dotted histograms give an idea of the local packing of atoms when neighbors are selected from both Li atoms and Si atoms. The types of defects in silicene and considered neighbors (in parentheses) are indicated in the captions in the margins of figures (a) – (d).

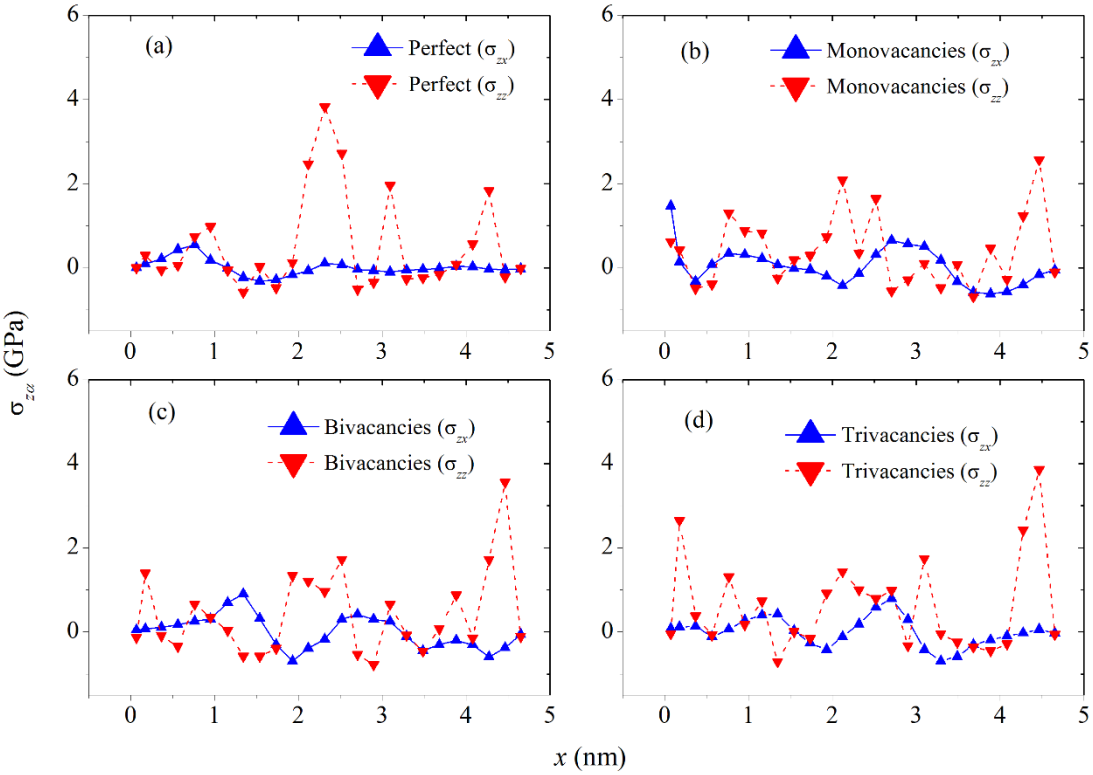

Figure 21 The distribution of the average σ_{zx} and σ_{zz} stresses in the sheets of silicene along the *ox* (zigzag) direction with limiting lithium filling of a silicene channel located on a Cu(111) substrate. Elementary areas are elongated along the axis *oy*. The types of defects in silicene and the stresses in question (in parentheses) are indicated in the captions in the margins of figures (a) – (d).

The distribution of SVP and SCP by the number of faces is shown in Figure 20. These distributions are quite compact with maxima lying in the interval $n = 6–8$ for SVP and $n = 7–11$ for SCP. On the whole, the n distributions for SVP and SCP are quite close, and the distributions obtained for a channel with perfect silicene walls are the most symmetrical.

The σ_{zz} and σ_{zx} stresses in the walls of a lithium-filled silicene channel located on the Cu (111) substrate are shown in Figure 21. As can be seen from Figure, the σ_{zz} stresses are always noticeably greater than the σ_{zx} stresses. In almost all cases, relatively strong bursts of local σ_{zz} stresses are observed, except for the case when the walls of the silicene channel contain monovacancies. Moreover, in channel walls made of perfect silicene, the highest surge σ_{zz} of stress occurs in the middle of the sheets, while for channel walls containing bi- and trivacancies, strong surges of σ_{zz} stress are found at the end of the sheets. Note that even the strongest local stress observed in the presence of trivacancies in silicene sheets is not critical, since it is no more than 26 % of the tensile strength of silicene (~15 GPa) [86].

Despite the fact that silicene on a copper substrate has not yet been obtained, thin films of silicon on copper have not only been created, but also investigated. Silicon films 250 nm thick were deposited on a copper substrate by radio frequency (RF) magnetron sputtering [87, 88]. For a small number of cycles, the copper-silicon anode showed a capacity above 3000 mAh·g^{-1}. However, as the number of cycles increased, the lithium-copper-silicon phase accumulated at the interface between silicon and copper. In addition, the plastic deformation in the copper substrate is increased. All this reduced the adhesion between the silicon film and the current collector and stimulated the destruction of the silicon film. Testing of silicon thin films deposited on metal substrates (e.g., copper or nickel) continues. Thin-film silicon contains nanometer-sized silicon elements. The resulting thin film silicon anodes are usually divided into nanocrystalline anodes and amorphous anodes [89]. As a rule, CVD is used to fabricate thin-film anodes from nanocrystalline silicon. To improve the performance characteristics of a thin-film anode, it is necessary to significantly increase the adhesion between the deposited silicon and the current collector.

3.3. Computer test of silicene-aluminum anode for lithium ion battery

The study of the anode material in the form of two-layer silicene on an aluminum substrate was carried out in [41]. An example of lithium intercalation into a silicene channel located on an Al(111) substrate is shown in Figure 22. By the time point corresponding to the Figure, 40 Li^+ ions were intercalated into the channel. The ions

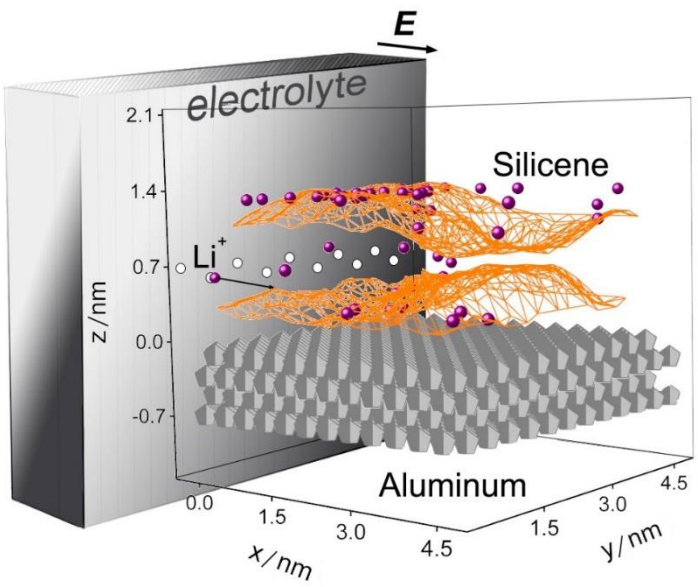

Figure 22 The channel, formed by perfect silicene sheets, on the substrate Al (111) during the intercalation process with lithium.

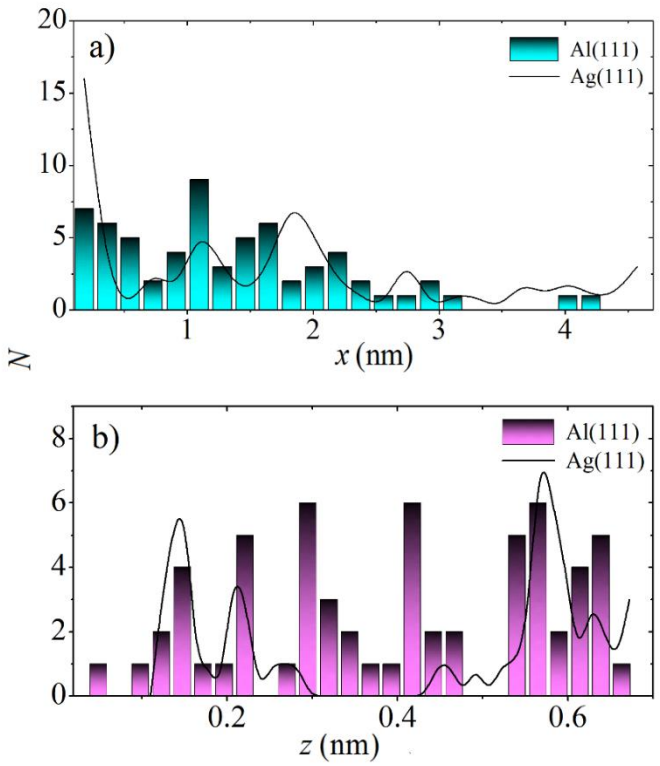

Figure 23 (a) horizontal (longitudinal) and (b) vertical profiles of lithium density in a silicene channel with bivacancies on Al(111) and Ag(111) substrates.

entered the outer surface of the top sheet of silicene through the gap between the impermeable side walls (not shown in the figure) and the edges of the sheets. As a result of deformation of the sheets, the volume of the channel made of perfect silicene decreased by 24 %, and for silicene with hexavacancies, by 32 %.

In the case of the presence of bivacancies in silicene, the number density profiles of the lithium-filled silicene channel look as shown in Figure 23. The horizontal lithium density profile in the channel (Figure 23 a) shows a large accumulation of Li atoms at the entrance ($x = 0$), while the vertical filling of the channel is denser in its middle part (Figure 23 b).

Let us divide the silicene channel containing monovacancies in its walls into parts equal in volume using the middle horizontal plane. The view from this plane to the top and bottom sheets of silicene is shown in Figure 24. It can be seen from the figure that there are 35 Li atoms in the zone of the upper sheet, while the number of Li atoms in the zone of the lower sheet is only 20. Not all monovacancies in both the upper and lower sheets have retained their original shape. Some of the monovacancies are dragging on. Instead, cyclic formations are formed, predominantly oval in shape, enclosing smaller holes. But larger holes can also be formed in comparison with the initial ones.

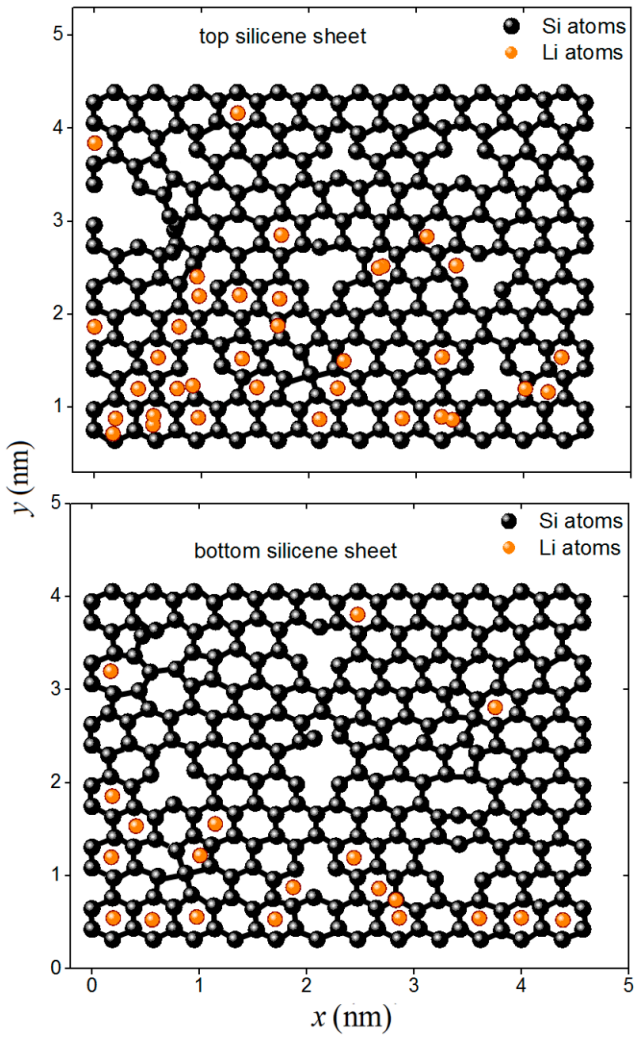

Figure 24. *Xy*-projections of the upper and lower sheets of silicene with monovacancies on the Al(111) substrate, at the time of complete lithiation (55 lithium atom was adsorbed on the silicene surface).

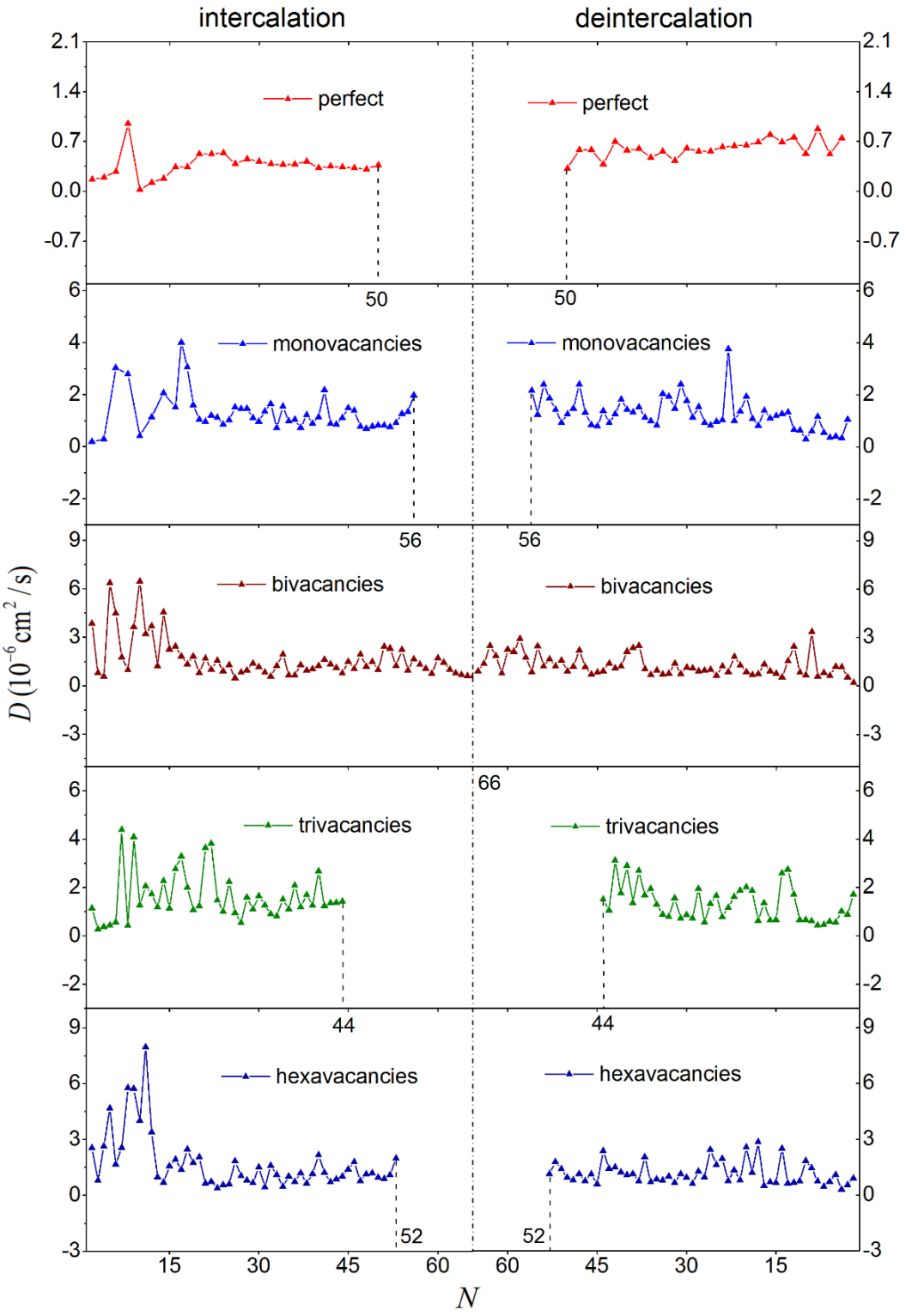

Figure 25 The coefficient of self-diffusion of lithium atoms in the process of intercalation (left) and deintercalation (right) in different silicene channels on the Al(111) substrate. The maximum achievable number of lithium atoms in the channel is marked with a dashed line.

The change in the self-diffusion coefficient of Li atoms in silicene channels is shown in Figure 25. The left side of each of the presented figures reflects the process of lithium intercalation, and the right side - the process of lithium deintercalation. The numbers in the figures show the limiting number of Li atoms filling each channel. After initial strong fluctuations in *D* during intercalation, its behavior becomes smoother, especially in the absence of vacancies in silicene sheets, because the number of collisions of the ion and Li atoms with the channel walls increases. As a rule, lithium deintercalation occurs with small fluctuations in the *D* coefficient. However, the

frequency of moderate fluctuations increases when the vacancy defects in the channel walls become large.

Sharp peaks in the angular distributions of the nearest geometric neighbors at angles of ~30 °, 60 °, 90 ° and less pronounced peaks at 120 ° indicate the location of some Li atoms above the centers of hexagonal rings in silicene (Figure 26). The peaks become less pronounced as the size of vacancy defects in the channel walls increases.

The stresses σ_{zx} and σ_{zz} appearing during intercalation and averaged over both sheets of silicene are shown in Figure 27. The stresses σ_{zz} are the strongest in the presence of trivacancies in the channel walls. Figures 27 a and 27 f show that the stresses in the perfect walls of the silicene channel located on the Al(111) and Ag(111) substrates are comparable. However, in these cases, different relationships are observed between the values of stresses σ_{zz} and σ_{zx}. Thus, aluminum and silver substrates have different effects on the stress distribution in the walls of the silicene channel.

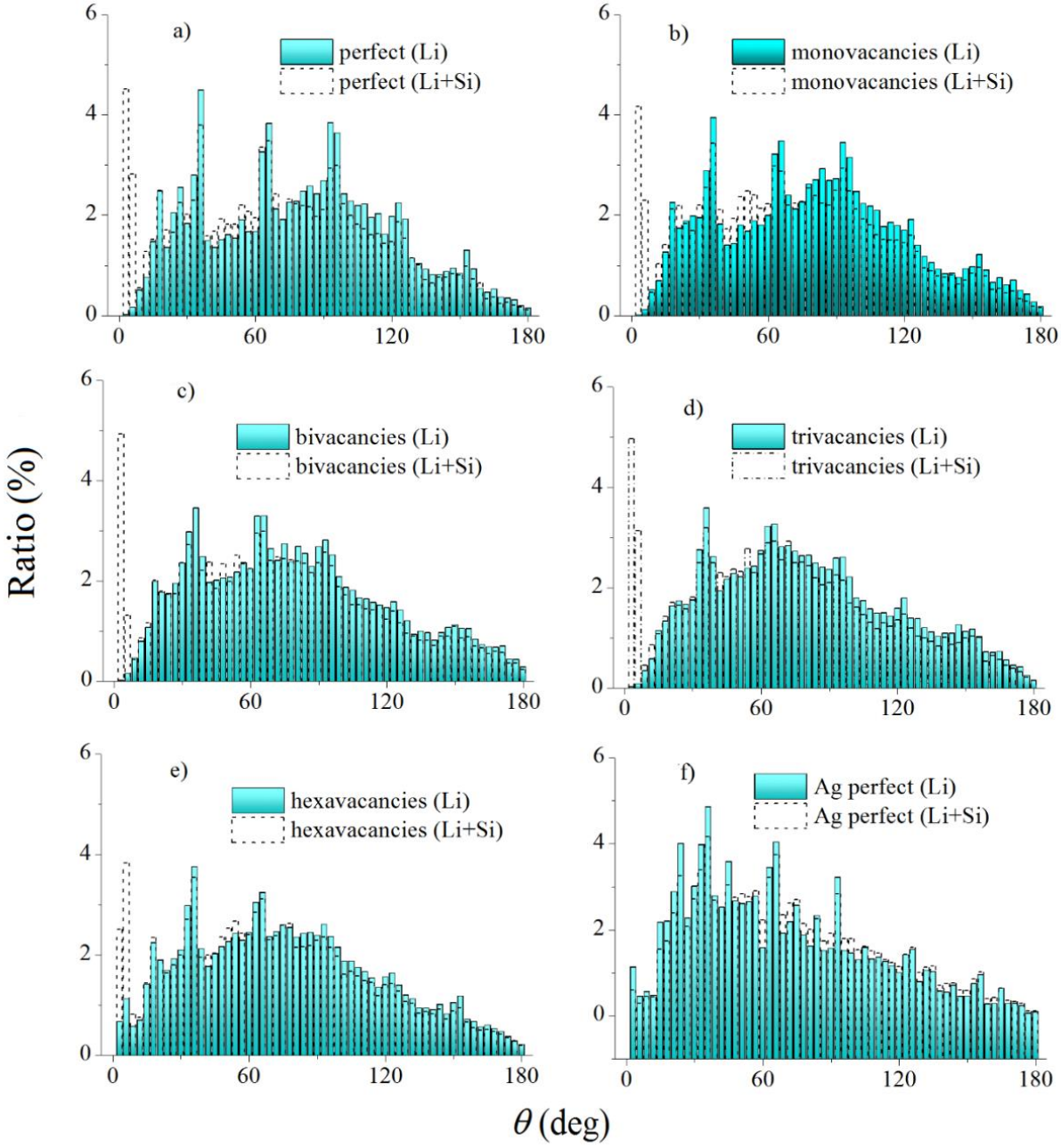

Figure 26 The angular distribution of the nearest neighbors for lithium atoms after instant when the silicene channel is completely filled: (a) – (e) on an Al(111) substrate, (f) on an – Ag(111) substrate. Solid (colored) histograms are obtained when neighbors are represented only by Li atoms, dotted histograms correspond to the case when neighbors are selected from both Li atoms and Si atoms. The types of defects in silicene and the neighbors under consideration (in parentheses) are indicated in the captions in the margins of figures (a) – (f).

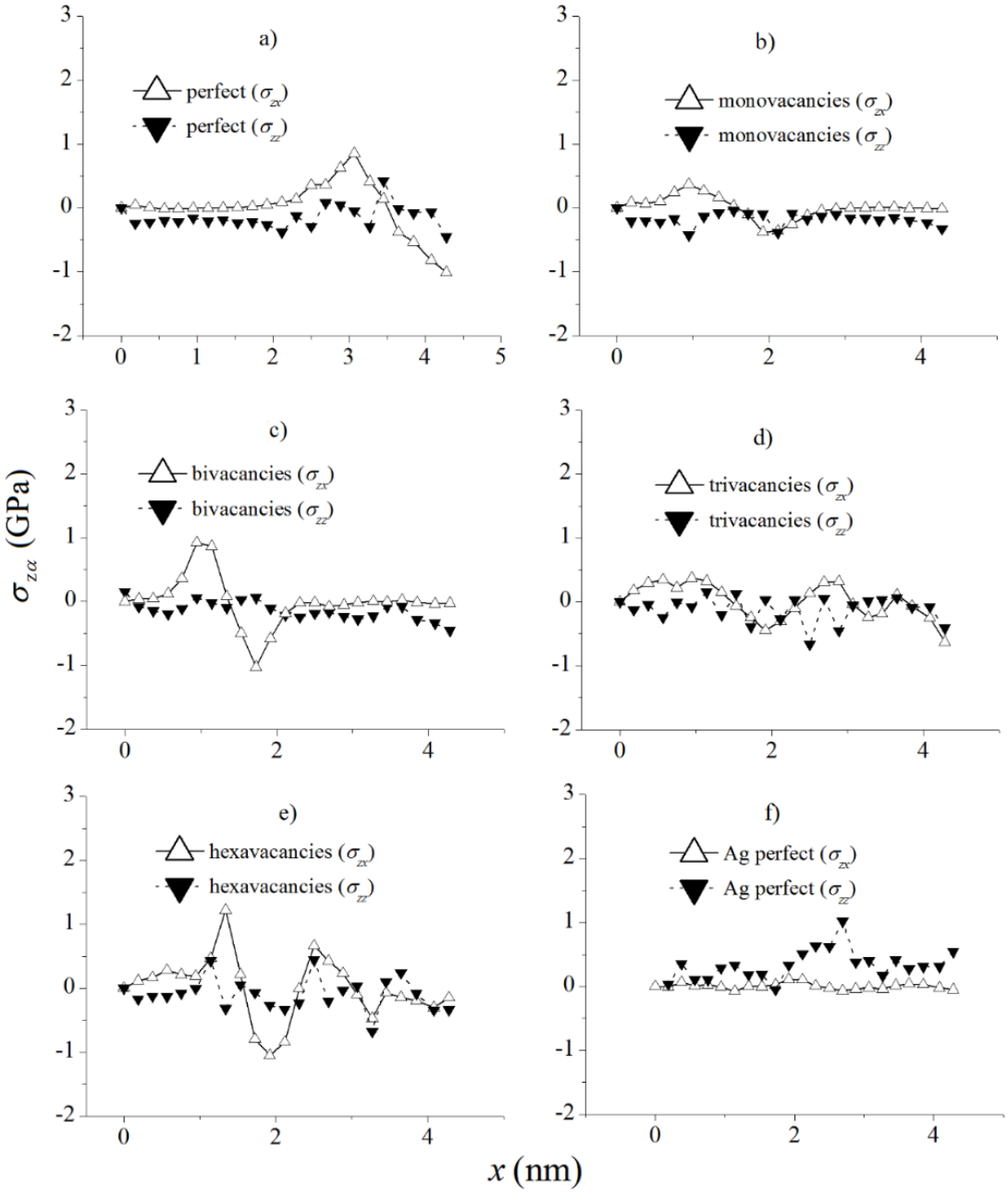

Figure 27 The distribution of the average σ_{zx} and σ_{zz} stresses in the sheets of silicene along the *ox* (zig-zag) direction when lithium is intercalated in a silicene channel located on an Al(111) substrate. Elementary platforms are elongated along the axis *oy*. The types of defects in silicene and the stresses in question (in parentheses) are indicated in the captions in the margins of figures (a) – (f).

Aluminum has a number of important qualities that make it a candidate for use as an anode active material. Such qualities are relative cheapness, wide distribution in nature, and low weight. However, aluminum easily reacts with lithium to form several phases: LiAl, Li_3Al_2, Li_2Al, and Li_9Al_4. At operating temperatures LIBs, when Al is fused with Li, the β-LiAl phase is formed [90]. Therefore, the use of aluminum as an active element of the anode is unpromising. However, the stable oxide layer on aluminum makes it possible to successfully use it as a current collector [91]. It was found that by obtaining the Li_9Al_4 compound with the electrode completely filled with lithium, it is possible to achieve the theoretical capacity of the aluminum anode (2235 mAh·g^{-1}) [92]. If the formation of such a compound is prevented, then the service life of the aluminum anode can be significantly extended. Thus, the coating of aluminum nanoparticles with a TiO_2 shell makes it possible to achieve a capacity of 650 mAh/g after 500 cycles.

3.4. Computer study of properties of silicon thin films on graphite

MD modeling of thin silicon films (including silicene) on graphite and the motion of a Li^+ ion along a silicene channel on graphite was performed in [93–95]. The properties of two-layer silicene on graphite were studied in the presence of a lithium ion moving along a silicene channel under the action of an electric field. In [93, 94], in the MD model, the possibility of the existence of a Si(001) film of crystalline silicon 2.2 nm thick and two-layer silicene with an interplanar distance of 0.2481 nm [44] on graphite at a temperature of 300 K was considered. Figure 28 shows the configurations of the studied films on a graphite substrate, obtained by the time of 200 ps. As can be seen from Figure, neither film was destroyed, and the distance between each of them and the graphite substrate remained the same (0.222 nm). At the same time, not only the studied silicon films, but also the graphite substrate underwent structural relaxation. Moreover, the adhesion between the substrate and silicene (0.15 eV/atom) turned out to be stronger than that with the Si(001) film (0.11 eV/atom). DFT calculations show that the difference in adhesion energy between silicene and graphite formed by three and four graphene sheets is less than 1% [x15]. Therefore, when the modeling silicene on a graphite substrate is carried out, it is sufficient to restrict ourselves to a three-layer thickness of graphite.

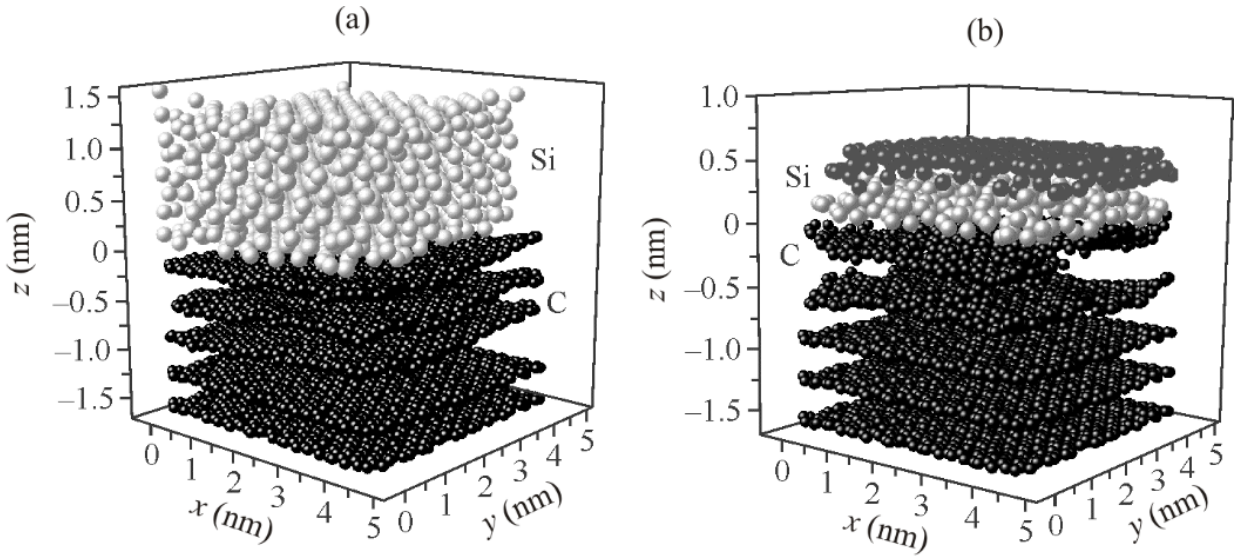

Figure 28 System configuration: Si(001) film on graphite (a) and bilayer silicene on graphite (b) for the time instance of 200 ps.

To check the crystallinity of the Si(001) film and preserve the silicene structure, the radial distribution function g(r) for the Si atom closest to the center of the sheet (or sheets) adjacent to graphite was calculated (Figure 29). In both cases, the function $g(r)$ was calculated for the silicon layer(s) closest to the substrate; for the bottom sheet of silicene (consisting of 300 atoms) and for two (001) layers of Si film, each containing 128 atoms. The sharp peaks of the $g(r)$ function indicate the retention of the crystal structure in films of both types. However, each of the films had its own structure, so that the intensity ratios of the first four peaks $g(r)$ for the lower silicene sheet (1 : 0.46 : 0.30 : 0.23) differ strongly from the intensity ratios of the corresponding part of the Si(100) film (1 : 0.75 : 0.54 : 0.37). The validity of this difference follows from the fact that the honeycomb structure of silicene is fundamentally different from the structure of crystalline silicon.

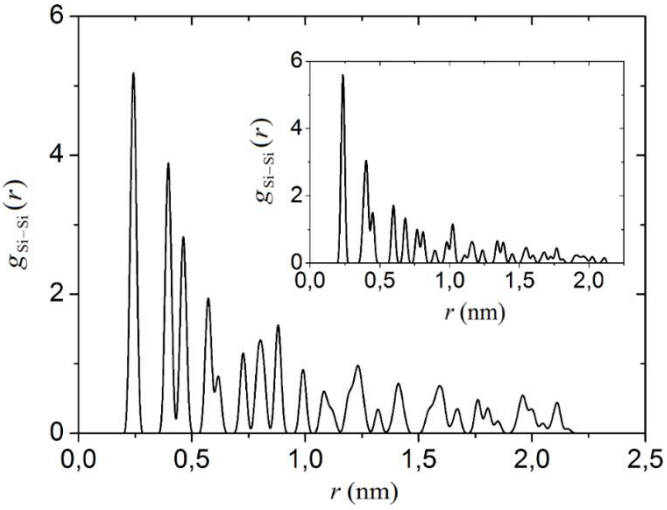

Figure 29 Radial distribution function for the central atom of the lower (256 atomic) Si (001) film on graphite; the inset shows RDF for the silicene sheet on graphite.

The passage of the Li^+ ion through the silicene channel located on the graphite led to distortion (both in the vertical and horizontal directions) of the silicene sheets, the *xy* projections which in the presence of trivacancies in them are shown in Figure 30 [95]. As can be seen from Figure, the defects in the bottom sheet of silicene are distorted more than the defects in the top sheet. In the lower sheet of silicene, the number of pores increased, but they became smaller. Atoms with two dangling bonds also appeared in the bottom sheet. Thus, due to the lattice incompatibility of graphene (graphite sheet) and silicene, the structure of the defective silicene sheet that has contact with graphite changed more than the structure of the top silicene sheet.

The Li^+ ion moving inside the silicene channel in an external electric field performs a zigzag motion, passing from one channel wall to another (Figure 31). In this case, the channel walls are subject to significant vertical deformation.

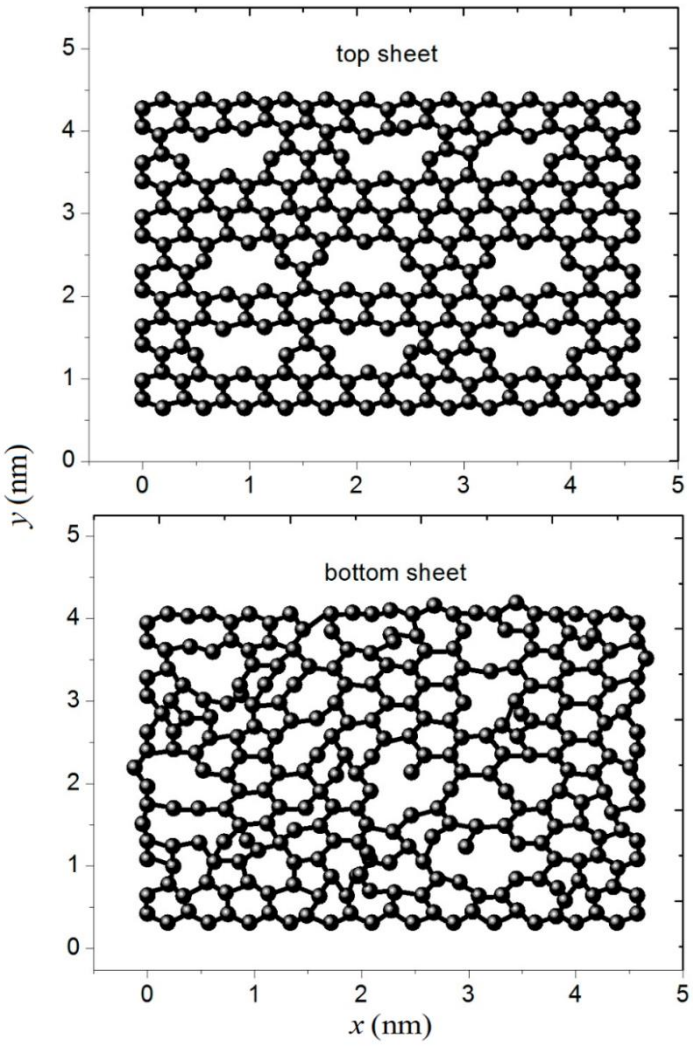

Figure 30 *Xy*-projections of the upper and lower sheets of silicene with trivacancies on the graphite substrate, with an interlayer gap of 0.75 nm and at the time of 100 ps.

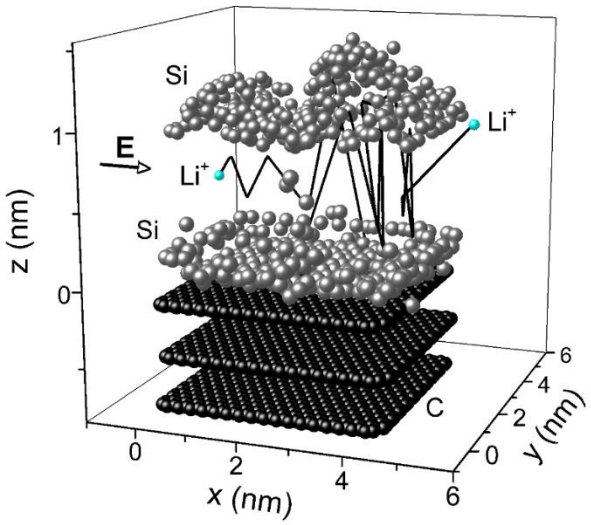

Figure 31 The configuration of the system "coupled sheets of silicene with bivacancies on graphite" with the initial gap between sheets h_g = 0.80 nm is shown together with the trajectory of the lithium ion motion along the channel during a time of 32.5 ps; a constant electric field **E** acts along the 0*x* axis.

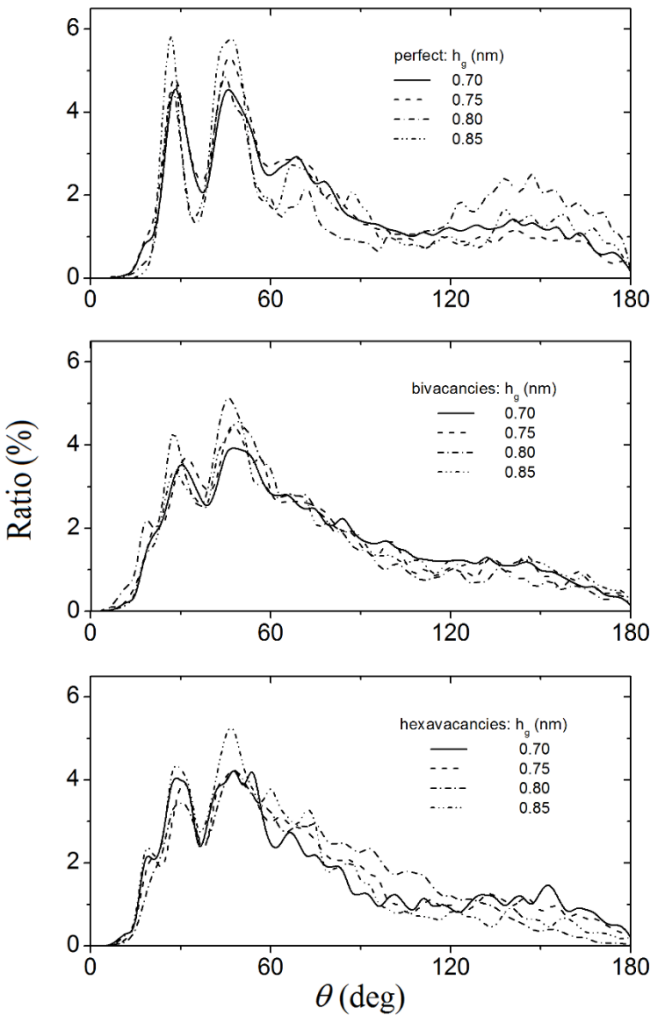

Figure 32 Angular distributions for the geometric neighbors of the lithium ion during its motion along various silicene channels on the graphite substrate.

Therefore, an ion moving along the channel can be used as a probe for studying the structure of the channel walls. In this case, the tool used to determine the state of the channel wall is the analysis of statistical distributions obtained for the elements of Voronoi polyhedra with the center located at the center of the lithium ion.

Polyhedra whose faces are formed from Si neighbors for the Li^+ ion were built every 1000 time steps. Statistical distributions were obtained by considering from 600 to 1000 polyhedra. Figure 32 shows the angular distributions constructed on the basis of considering the relative position of neighbors, determined by constructing such polyhedra. At the same time, Figure 32 reflects only the cases when the walls of the channel were sheets of perfect silicene, as well as silicene containing bi- and hexavacancies. As can be seen from Figure, the shape of the resulting angular distribution depends on both the state of the walls and the gap h_g of the channel. The peak intensities in the vicinity of the 30 ° and 45 ° angles increase with h_g. However, an increase in the size of vacancy defects slows down the growth of the intensity of these peaks. In the angular distribution for a channel with perfect walls and a large gap (0.85 nm), a dome is formed in the range of angles from 120 ° to 180 °, which can be due to the strong curvature of the walls of such a channel. Figure 33 shows the face distributions of simplified polyhedra. These polyhedra do not have small facets, which most often appear as a result of small-scale thermal fluctuations [96]. In other words, these distributions can be used to identify more probable geometric neighbors located in the environment of the Li^+ ion. Nevertheless, in contrast to the angular distribution (shown in Figure 32), here it is not possible to establish a regularity in the dependences of the number of the most probable faces on the gap size of the silicon channel and the size of defects in silicene sheets.

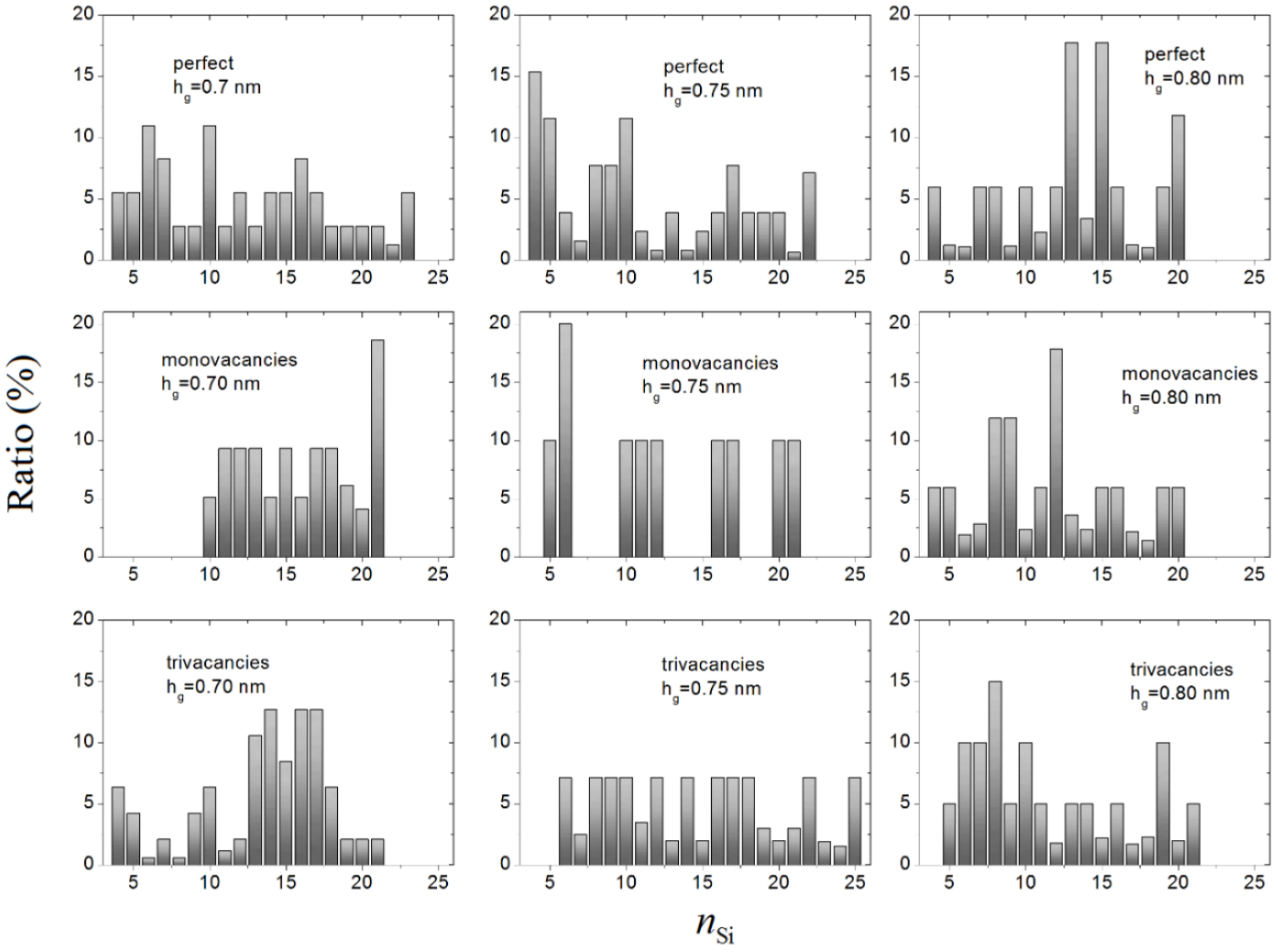

Figure 33 Frequency of occurrence of the number n_{Si} of Si atoms included in the more probable geometric neighbors of the Li^+ ion during its motion along a perfect silicene channel and a channel whose walls contain different vacancy defects; h_g is the width of the gap of the silicene channel which is on the graphite substrate.

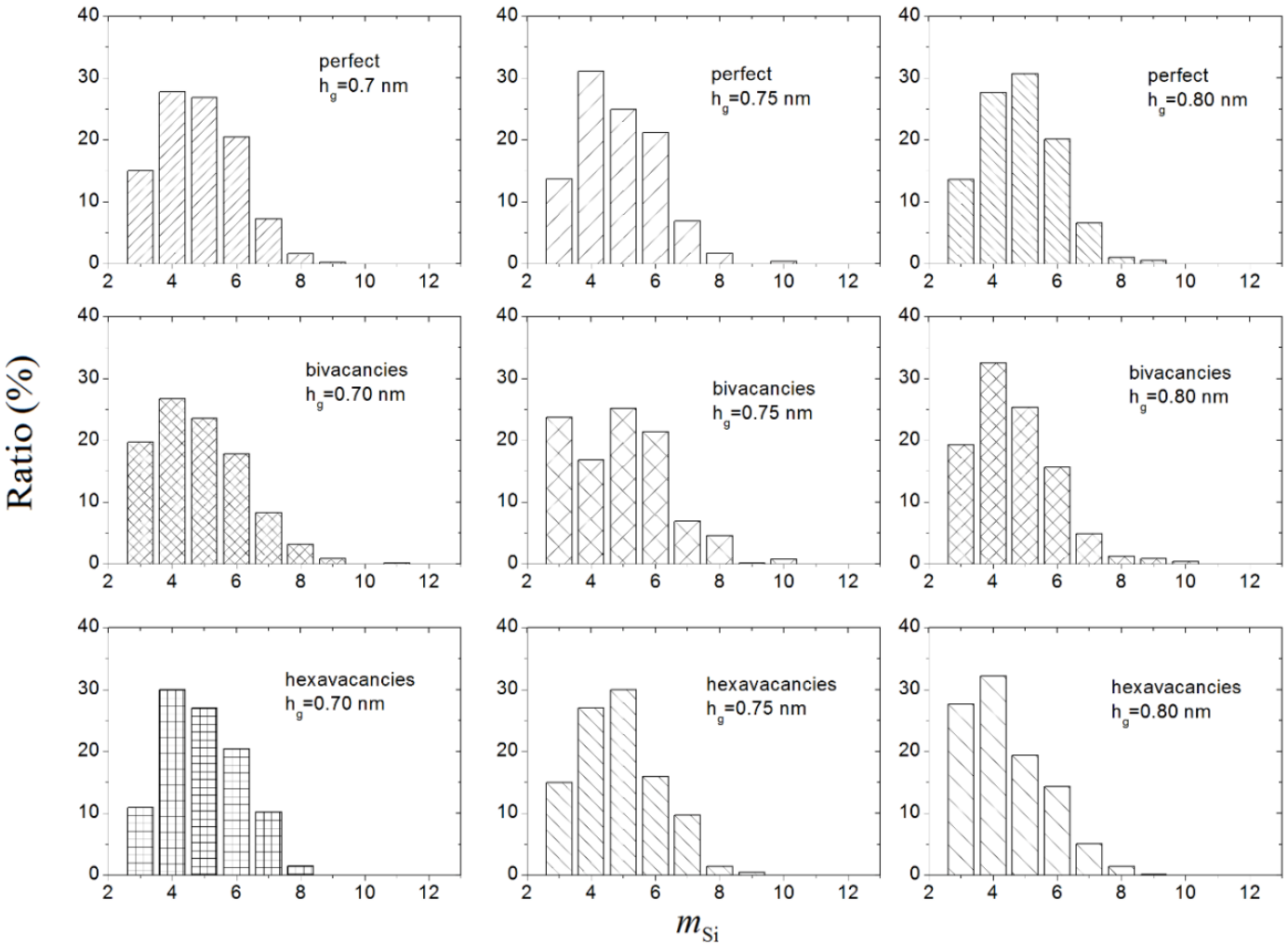

Figure 34 The number of Si atoms that form the averaged rings around the Li^+ ion in channels with different gaps, the walls of which contain various defects; all channels are on the graphite substrate.

The transition to the consideration of simplified polyhedra made it possible to more easily interpret the statistics of m-membered rings or the distribution of faces over the number of sides. Face distributions of simplified polyhedra by the number of sides characterizing local Si structures encountered by a moving Li^+ ion are shown in Figure 34. It can be seen that four-membered rings are predominant when the channel gap has a size of 0.70 nm, regardless of the presence of defects in the channel walls. In other cases, both four- and five-membered Si-rings are most often encountered when observed from the center of the Li^+ ion in the directions of geometric neighbors. In most cases, the expansion of the channel increases the likelihood of observing five-membered rings.

Stresses σ_{zz} are the most significant stresses acting on the walls of silicene channels, along which a lithium ion moved under the action of an electric field with a strength of 10^5 V/m. Here, the influence of the channel gap and the type of defects in the walls of the silicene channel on the stress distribution along its length (axis *ox*) is clearly not traced (Figure 35). The normal force acting on the channel walls and creating σ_{zz} stress is directed downward due to the attraction of the two-layer silicene to the graphite. Therefore, σ_{zz} stresses are almost always negative. The maximum absolute value (1.65 GPa) of the fluctuating stress σ_{zz} appears in the case of a silicene channel with perfect walls and a gap h_g = 0.85 nm. This value is two or more times smaller than the corresponding characteristics observed when filling silicene channels on metal substrates with lithium and is ~12 % of the tensile strength of silicene [97]. Thus, the movement of a lithium ion through silicene channels is not associated with the formation of dangerous mechanical stresses in the channel walls.

Scanning the walls of the silicene channel showed that the silicene sheets have a specific structure that is not similar to the structure of three-dimensional ordered or disordered materials. Two distinct peaks are observed in the angular distributions of the nearest Si neighbors

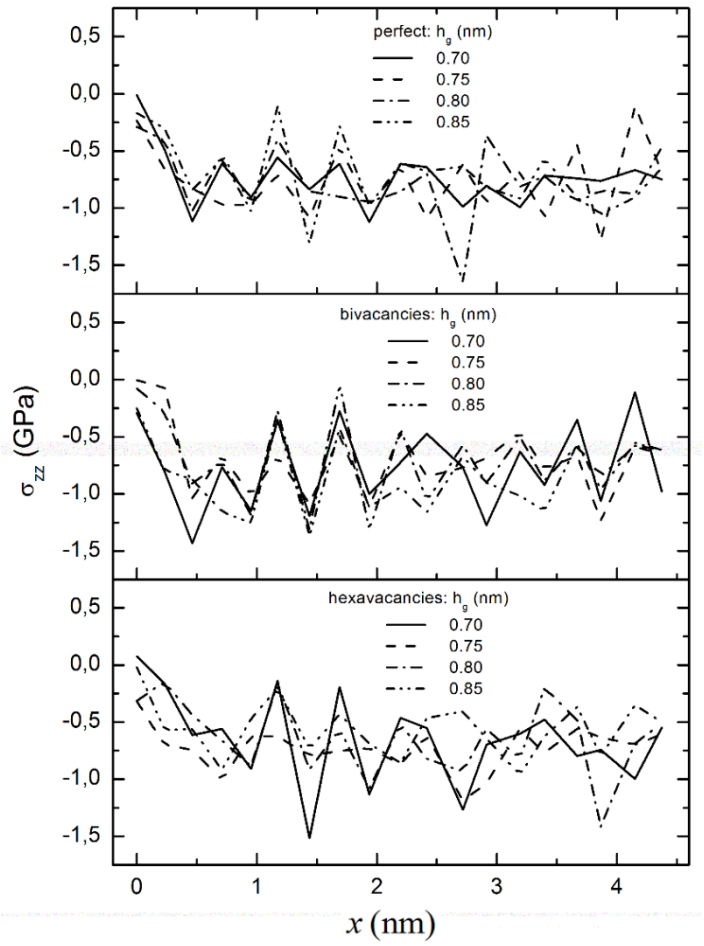

Figure 35 Distribution of stress $\sigma_{zz}(x)$ averaged over both sheets of the perfect and defective silicene along axis 0*x* (zigzag direction) coinciding with the direction of the electric field strength at different gaps; silicene sheets are on the graphite substrate.

detected with the help of a lithium ion moving in an electric field along the channel.

The intensity of these peaks is affected by both the channel gap and the type of defects in the walls of the silicene channel. The transition to the analysis of simplified polyhedra makes it possible to establish that for the Li+ ion in the silicene channel, it is possible to consider a neighborhood with the number of Si atoms from 4 to 21. In this case, m-membered Si rings containing from 3 to 8 members in nearest neighbor directions are found. The σ_{zz} stresses are the most significant stresses that exist in the channel walls. However, even in the presence of hexavacancies in the channel walls, these stresses cannot lead to the destruction of silicene sheets. Thus, two-layer silicene on a graphite substrate may be a candidate anode material for LIBs.

3.5. Lithiation of two-layer silicene on the SiC substrate

Silicon carbide is a heat-resistant material that has found application in high-temperature rectifier diodes and field-effect transistors, light-emitting diodes, and ultraviolet radiation detectors. SiC is used for the manufacture of heat and radiation resistant integrated circuits, as well as for the creation of microwave devices.

It was hoped that the combination of Si and C atoms in silicon carbide would make it possible to create a high-performance anode material from it. In fact, it turned out that the capacity of such an anode with respect to lithium is not high enough [98]. Ab initio MD calculations suggest that layered SiC is a suitable anode material for use in LIB. Indeed, this material is characterized by structural strength, high electronic conductivity, low diffusion barrier (0.40 eV), and relatively high capacity (699 mAh·g^{-1}) [99]. Calculations show that SiC is a semiconductor with an indirect band gap, which has a width of 2.35 eV [100]. After complete lithiation, SiC passes into the metallic phase. SiC retains its structure after the adsorption of Li atoms. In this case, the open circuit voltage is 1.5 eV. Such a voltage appears to be unfavorable due to the deposition of lithium metal, the formation of dendrites, and the formation of a solid electrolyte boundary. These factors lead to battery short circuits and other problems. It is quite logical to try to increase the anode capacitance by combining the SiC film with two-layer silicene. It is this variant of the combined anode that was considered in [101, 102].

In all previously considered cases, the silicene channel was filled with lithium in the horizontal direction; Li^+ ions were launched into the channel parallel to its walls. In [101], along with the horizontal method of filling the channel with lithium, the corresponding vertical method was considered. In the vertical method, Li^+ ions are directed into the silicene channel perpendicular to its walls in the presence of vacancy-type defects in the channel walls.

Figure 36 shows a scheme for performing a computational experiment with vertical and horizontal filling of a silicene channel with lithium. The inset at the bottom of the figure shows a fragment of the upper layer of the SiC substrate on an enlarged scale. The plane of the substrate closest to the silicene is formed by hexagons with C atoms at the sites. The plane with Si atoms is located below the carbon plane. When the silicene channel was filled vertically, the launched lithium ions were initially located on the *xy* plane located 0.6 nm above the upper wall of the channel. In the case of horizontal filling, the Li^+ ions were initially located in the *zy* plane, which was at a distance of 0.3 nm from the entrance to the channel. The ions were directed into the channel under the action of an electric field of the corresponding direction. The strength of the external electric field was 10^4 V/m. Ions were launched every 10 ps.

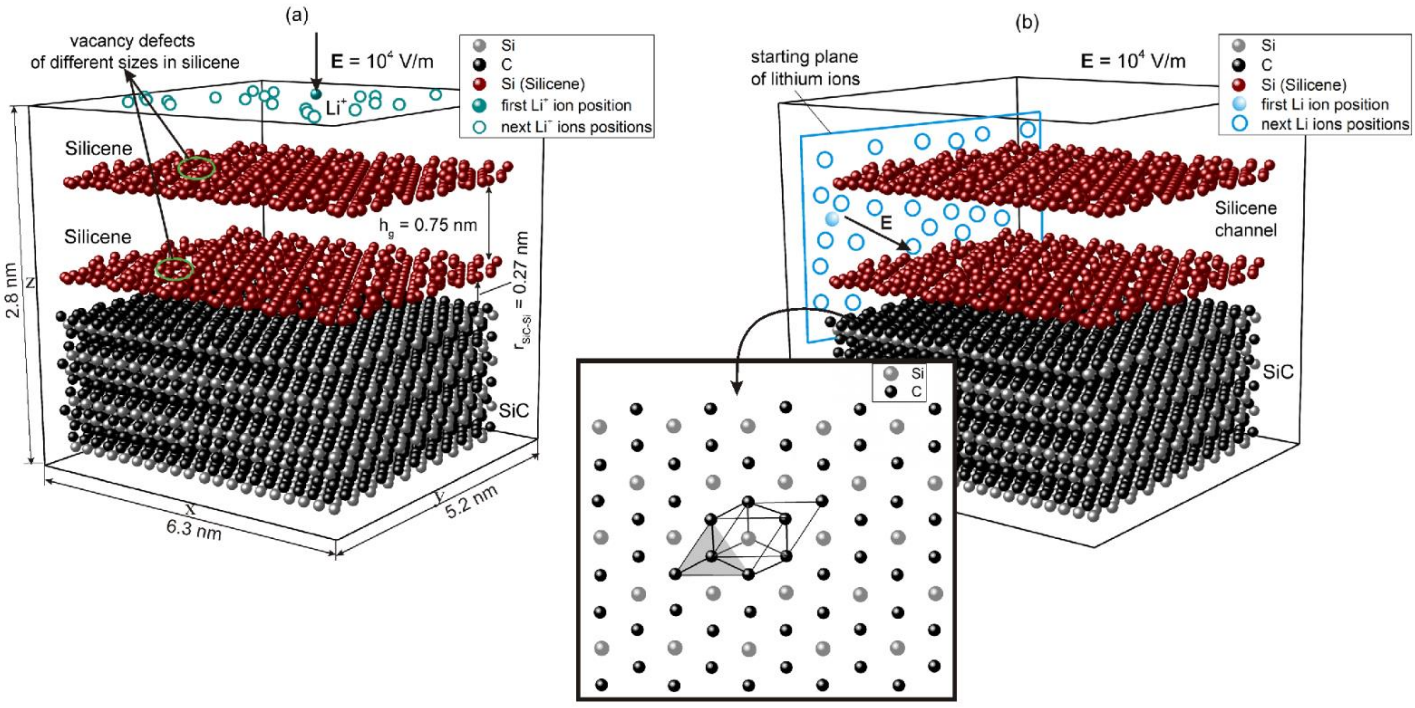

Figure 36 Schematic representation of the initial configurations (time moment $t = 0$ ps) of the simulated systems in the case of (a) vertical and (b) horizontal filling of the silicene channel with lithium ions; the silicene sheets are on on the SiC substrate and have vacancies of given sizes; the ions initial sites (open circles) belongs to (a) *xy* and (b) *zy* surfaces; the insert shows a part of the substrate upper layer and a unit cell.

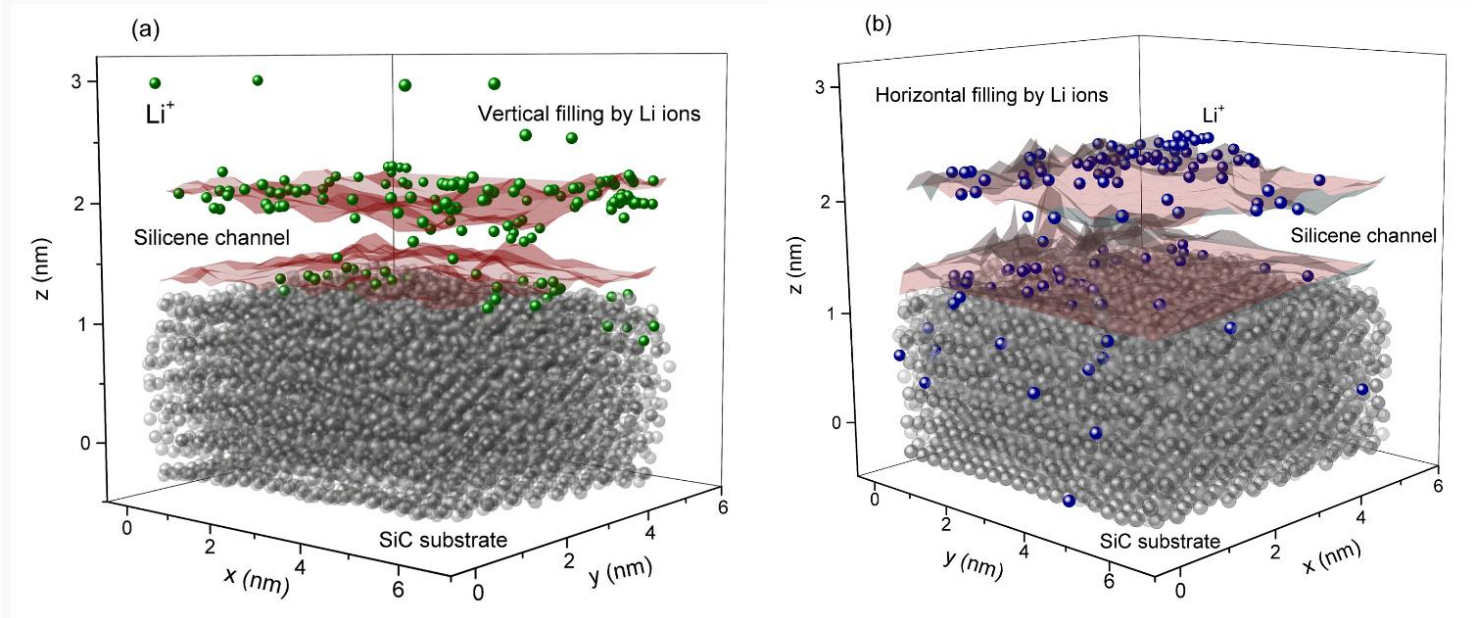

Figure 37 Configurations of intercalated systems after launching 151 Li^+ ions to inject them into the silicene channel located on the SiC substrate; the intercalation is performed: (a) vertically and (b) horizontally; silicene sheets are modified with bivacancies; for convenience of visualization, the silicene sheets are represented as surfaces and the SiC substrate is shown as a shadowed object.

Figure 37 shows the configurations of vertically and horizontally filled anodes related to the time of 1.51 ns. In the case of vertical filling, by this time, 41 Li atoms directly entered the channel, while 96 Li atoms remained outside, including those deposited on the upper silicene sheet. When ions were launched in the horizontal direction, 73 Li atoms got inside the channel and 65 Li atoms remained above or on the surface of the upper silicene sheet. In addition, in this case, several (13) Li atoms penetrated into the SiC substrate, which was not observed when the channel was filled vertically. In both ways of filling the silicene channel, the Li atoms that got inside the channel

Table 1 – Average values of the lithium self-diffusion coefficients.

Vertical lithiation		Horizontal lithiation	
Vacancy type in silicene	D_{Li}, 10^{-5} cm²/s	Vacancy type in silicene	D_{Li}, 10^{-5} cm²/s
bivacancy	3.16	bivacancy	4.06
trivacancy	2.88	trivacancy	3.72
hexavacancy	3.05	hexavacancy	4.80

or located outside on the surface of the top sheet of silicene were predominantly located above the centers of the six-membered Si rings.

The behavior of the self-diffusion coefficient of Li atoms interacting with the anode during intercalation is shown in Figure 38. As can be seen from Figure, a strongly oscillating behavior of the coefficient *D* is observed both in the cases of vertical and horizontal filling of the channel with lithium. However, the number of stronger *D* oscillations is usually higher in the case of horizontal channel filling. The frequency and intensity of the oscillations of the coefficient *D* also depend on the type of defects in the walls of the silicene channel. The intensity of the oscillations decreases when there are trivacancies in the channel walls. Perhaps this is due to the complex, non-smooth relief of the boundaries of these defects, which, to some extent, can "quench" strong oscillations of *D*. With any method of filling the channel with lithium, the frequency of strong oscillations of *D* increases in the presence of hexavacancies in the channel walls, which have smoother boundaries compared to three – and bivacancies. The dependence on the method of filling the channel with lithium is expressed in the fact that at the final stage of intercalation, for any type of defects in silicene, the intensity of the oscillations decreases significantly in the case of vertical filling of the channel. Perhaps this is due to the smaller number of Li atoms falling directly into the channel with this method of intercalation, since the frequency of collisions of Li atoms with the channel walls in this case can be lower.

The average self-diffusion coefficients of Li atoms in the considered anodes presented in Table 1 can be affected by the substrate material, the number of silicene sheets, and the size and number of defects contained in the silicene sheets. Based on DFT calculations, it was shown in [103] that the coefficient of self-diffusion of Li atoms on a free-standing silicene sheet at a temperature of 300 K is $5 \cdot 10^{-5}$ cm²/s.

The statistical geometry method was used to study the packing structure of lithium atoms in the anodes under consideration. The distribution of VP by the number of faces for lithium packings obtained by horizontal and vertical filling silicene channels with various types of defects in their walls is shown in Figure 39. The common thing for the obtained n-distributions is that their maxima fall on $n = 4$. As a rule, the horizontal filling of the anode with lithium leads to a shorter length of the *n* distributions. In other words, in this case, packings with a higher degree of crystallinity appear. This is connected to a certain extent with a large number of Li atoms inside the channel. However, in the presence of trivacancies in the channel walls, the length of *n* distributions for both methods of filling the anode with lithium is the same, and the intensity of the n-spectrum at $n = 4$ is higher in the case of vertical filling.

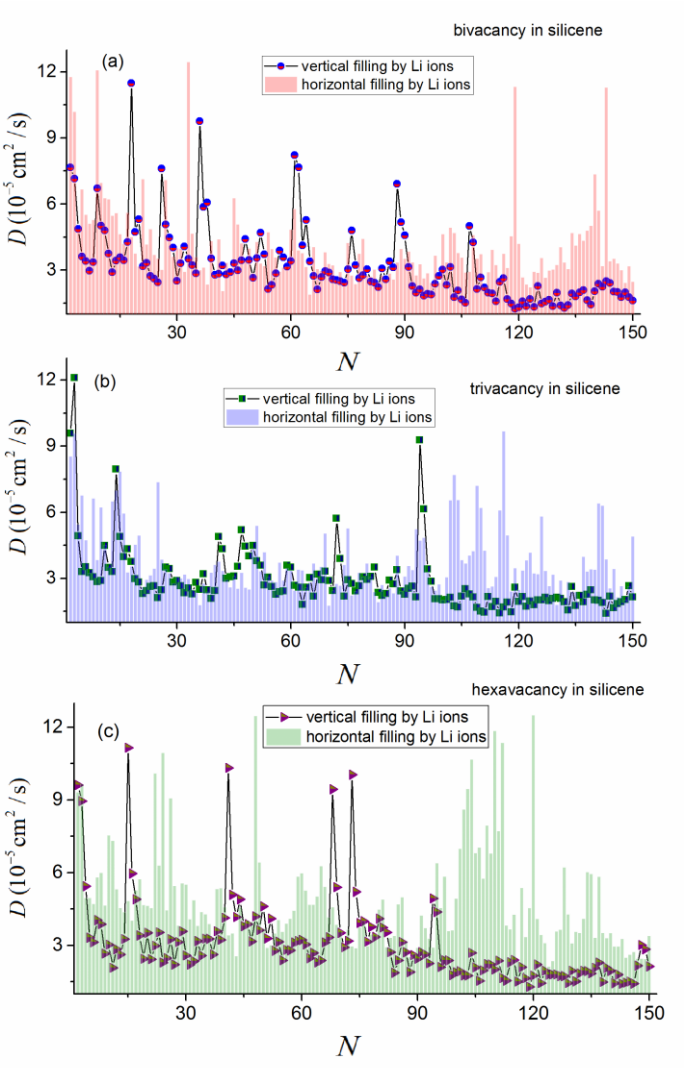

Figure 38 Self-diffusion coefficients of lithium atoms in systems "defective silicene channel located on the SiC substrate" with various defects in the channel walls during vertical (lines and dots) and horizontal (histograms) intercalation of lithium.

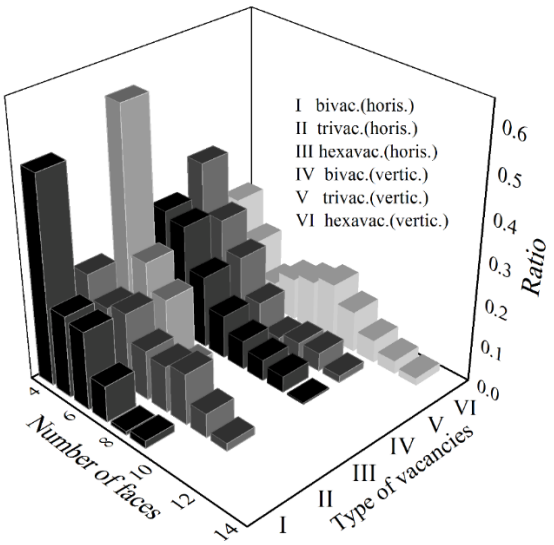

Figure 39 Distribution of Voronoi polyhedra according to the number of faces constructed for lithium packings in the silicene/SiC systems with horizontal and vertical intercalation; the two-layer silicene contained bi-, tri-, and hexavacancies.

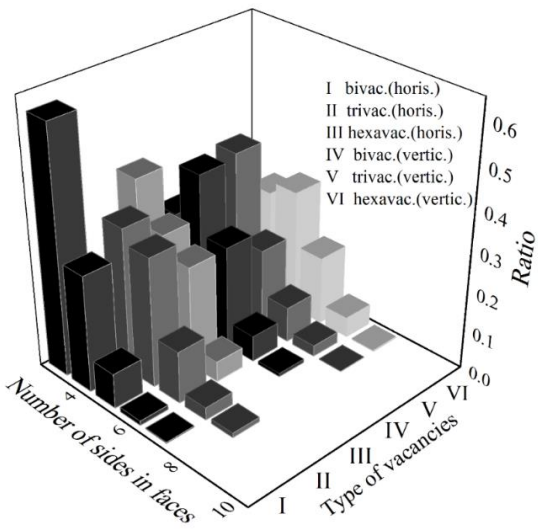

Figure 40 Distribution of faces of Voronoi polyhedra according to the number of sides; the study is carried out for lithium packiges in the silicene/SiC systems with horizontal and vertical intercalation; the defects in bilayer silicene are bi-, tri-, and hexavacancies.

In the case of horizontal filling of the anode with lithium, the maximum in the distribution of faces over the number of sides falls at $m = 3$, when bi- and hexavacancies are present in the channel walls, and at $m = 4$, when there are trivacancies in silicene (Figure 40). When the anode is filled vertically with lithium, the maximum of m-distribution corresponds to the value $m = 4$ in the presence of bi- and trivacancies in the channel walls and $m = 5$ when the defects in silicene are hexavacancies. All m-distributions for given bulk packings of Li atoms have a sufficiently large extent (up to $m = 8$), since they are derived for true (not simplified) VPs. Accounting for small-scale thermal fluctuations in the obtained m-distributions complicates the structural analysis. Nevertheless, the appearance of fifth-order rotational symmetry in the presence of hexavacancies in the walls of a vertically filled silicene channel indicates an increase in irregularity in such a packing of Li atoms.

The angular distributions of the nearest geometric neighbors characterizing the packings of lithium in "silicene/SiC" anodes, obtained by filling the electrodes horizontally and vertically with lithium, are shown in Figure 41. Angular distributions are presented here only for cases where the channel walls contain bi- and hexavacancies.

The corresponding distributions for lithium-filled channels with walls containing trivacancies have a form similar to the presented distributions. All these distributions reflect the case when the packing of Li atoms is formed from a mixture of irregular and regular packings. Packing regularity is expressed in the presence of individual sharp peaks in the spectra, which in general form represent irregular packing. The highest sharp peaks are present in the vicinity of angles 36 ° and 63–66 °. Such peaks are more pronounced for cases where bivacancies are present in silicene, especially when the anode is filled vertically with lithium. In the same cases, these distributions contain less pronounced peaks in the vicinity of the 120 ° angle. Most of the discussed peaks are formed from the location of some Li atoms above the centers of the six-membered silicon rings. On the whole, there are more similarities than differences in the structure of lithium packings obtained by horizontal and vertical intercalation.

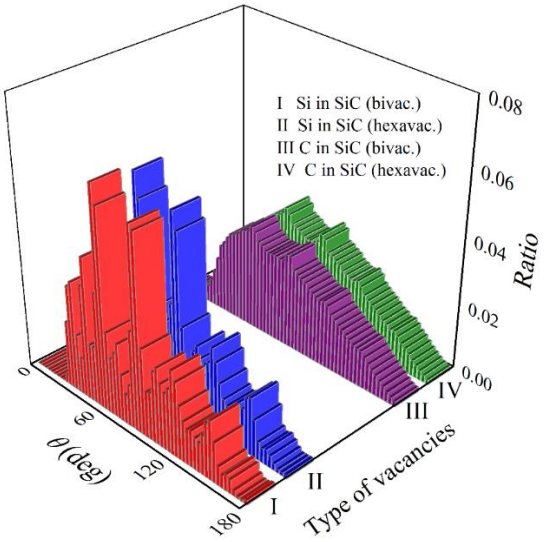

Figure 41 Angular distribution of nearest geometric neighbors for lithium packings in silicene/SiC systems with horizontal and vertical intercalation; the data are presented for cases where the two-layer silicene contained bi- and hexavacancies.

Table 2 – Adhesion energy between single-layer silicene and metal (Ni, Cu, Al, Ag, Au) and non-metal (graphite, silicon carbide) substrates (eV/ elementary cell).

Parameter	Ni	Cu	Al	Ag	Au	C	SiC
E_{adh}	2.9	2.0	1.1	1.2	1.0	0.3	1.1–1.7

It is of interest to compare the structures of the Si and C subsystems of silicon carbide after filling the "silicene/SiC" anode with lithium using the method of statistical geometry. As an example, we use for this the results obtained when the anode in question is filled vertically with lithium. In this case, the analysis of topological properties was performed for simplified Voronoi polyhedra (SVP). In Figure 42, the distributions of faces by the number of sides for both subsystems are presented, when bi-, tri-, and hexavacancies served as defects in the walls of the silicene channel. The maximum of m distributions for Si-subsystems falls on $m = 4$, and for C subsystems – on $m = 5$. According to this feature, as well as the shape of the angular distributions of the nearest geometric neighbors determined using VP, the C subsystem turns out to be more disordered than the Si subsystem [104].

DFT calculations show that the adhesion energy between single layer silicene and Ni(111) substrate is much higher then E_{adh} between perfect silicene sheet and other metal substrates (Table 2) [105, 106]. The adhesion energy between single-layer silicene and graphite has the lowest value among all considered substrates [107]. The E_{adh} value between the silicene sheet and layered silicon carbide is not uniquely determined due to the continuous approach of Si atoms to the relaxing SiC substrate [108].

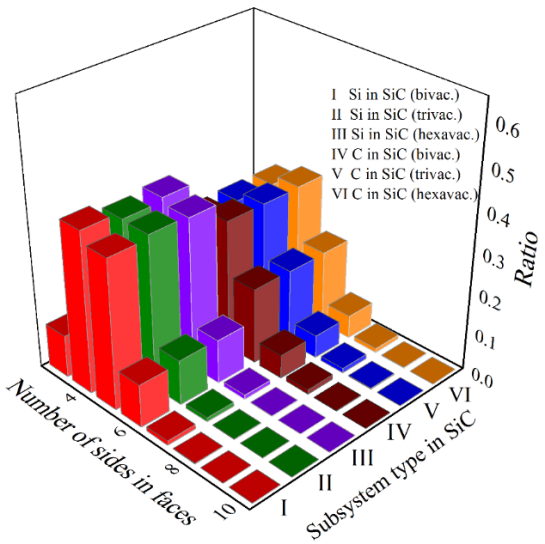

Figure 42 The distribution of faces of SVP by the number of sides constructed for the Si and C subsystems of SiC after the silicene/SiC system is vertically filled with lithium in 1.51 ns; the types of defects in silicene are indicated in parentheses.

The voltage profile during the discharge of a SiC element was calculated in [109] using ReaxFF simulation. This profile indicates the possibility of using SiC material as an electrode with a theoretical capacity three times higher than the corresponding capacity of a graphite electrode. The mechanism of lithium intercalation was considered in the framework of the analysis of charge transfer and the study of electronic conductivity. It is noted that the SiC layered material is suitable for use in LIBs as a fairly effective anode material. SiC, C/SiC, and Si/C/SiC samples were obtained by carbothermal synthesis and the addition of electrodeposited silicon fibers, and their electrochemical behavior in the LIB anode cell was studied [110]. Their Coulomb efficiency after 100 cycles was above 99 %. Significant efforts are required to test the combined "silicene/SiC anode" experimentally.

4. Discussion

To prevent a large increase in the volume of silicon during lithiation, silicon containing combined films were used as an anode. Higher capacitance and better capacitance retention than an amorphous silicon film are demonstrated by an amorphous Si/TiN film in which silicon nanoparticles were embedded in a TiN matrix [111]. The electrochemical characteristics of a multilayer Fe/Si film were studied, where Fe effectively suppressed the volume expansion of Si during cycling [112]. The Mg_2Si nanocrystalline film showed stable behavior during cycling, providing a reversible capacity of 2200 mA·h·g^{-1} for more than 100 cycles [113].

Metal substrates tend to overwhelm the outstanding properties of silicene. This problem can be solved, for example, by oxygen intercalation [114]. Other methods have also been used, such as the insertion of an atom-thick insulating sheet. A single layer of h-BN can serve as such a sheet [115]. In [116], it is proposed to synthesize quasi-free silicene on a thin CaF_2 epitaxial film, which can be formed on a Si(111) substrate. In the absence of a metal substrate, the doping of silicene can be controlled, as well as easy extraction and transfer to a convenient substrate, including for use in flexible electronics [117, 118]. Potential applications of silicene extend to the fields of energy storage and conversion [119], sensors, as well as use in medicine and biology [120].

The creation of microbatteries with 3D architecture has faced certain difficulties, including the uneven distribution of current and voltage, the complexity of spatial design due to the small size of the battery, and the need to develop conformal electrolytes with high conductivity. However, wireless devices that perform discovery, computing, and communication functions are

being intensively developed for a variety of applications, including wearable medical devices, continuous monitoring devices in the industrial sector, and remote environmental monitoring devices. Due to the widespread use of wireless sensor devices, the need for full-fledged 3D batteries in a miniaturized form has increased. The development of architectural design continues. An excellent tool for this is 3D printing, which allows for flexible dimensions and geometries, which should eventually lead to higher current densities [20].

Battery geometry and material properties have a decisive influence on the charge conduction path. Using finite element simulations, it was possible to show that the incorrect location of the electrodes creates an inhomogeneous current density, which leads to uneven use of the active material and partially unused electrodes [121, 122]. Many details of the processes that occur in batteries during operation can be established by numerical simulations. At the same time, the complexity of the battery architecture fades into the background. Electrochemical processes in three-dimensional microbatteries were studied by the finite element method both in the case of using liquid [121, 122] and solid electrolytes [123, 124]. The non-uniformity of the current density causes mechanical stresses that affect the material of the components and the performance of the LIBs. Numerical studies make it possible to quantitatively characterize this effect [12].

To improve poor kinetics and thermodynamic stability at the electrode-electrolyte interface, the appropriate interface must be carefully studied. In addition to improving conductivity, the electrochemical window of solid state electrolytes must be optimized to ensure reversible deposition and removal of charge carriers and reduce interfacial resistance. Currently, the electrochemical window of inorganic solid-state electrolytes has reached a value of 3 V, but the corresponding conductivity is quite low. Therefore, it is necessary to significantly improve the mechanism of ion transport. This can be achieved by optimizing the structure and compositional design of composite solid state electrolytes [8]. Thus, a composite solid electrolyte with a high content of inorganic filler should have higher electrical conductivity and electrochemical stability, as well as higher cyclic stability. At low temperatures, the aging of a lithium-ion cell is associated with the deposition of lithium metal on the anode [125]. At the same time, an increase in temperature is accompanied by an increase in the SEI layer on the anode and an acceleration of cathode destruction. These effects lead to a decrease in capacitance and an increase in internal resistance.

This review presents the work performed at the atomic level based on the developed molecular dynamics model. The computational developments discussed can first of all be extended to the description of electrochemical processes in microbatteries. The design of a microbattery with a silicene anode was proposed in [126]. In the review of the physicochemical processes of charging and discharging promising silicene anodes of a lithium-ion battery are considered. At the same time, the active two-dimensional material silicene was placed on metal (Ag, Ni, Cu, Al) and non-metal (graphite, silicon carbide) substrates. In all cases, the launch of ions and their extraction from the anode element (silicene channel) was carried out under the action of an external electric field. The occupancy of a silicene channel with lithium was studied depending on the type of vacancy defects (mono-, bi-, tri-, and hexavacancies) present in its walls for each type of substrate under study. The self-diffusion coefficients of lithium atoms entering the silicene channel during charging of the anode element and leaving it during discharging are calculated. The value of the self-diffusion coefficient of lithium atoms largely determines the battery charging rate. The morphology of the anode element was studied, as well as the change in its volume during cycling, the change in the roughness of silicene sheets after filling the channel with lithium was established. Particular attention is paid to the study of lithium atom packings obtained by filling the silicene channel with lithium and by removing lithium from the anode element. The structure of lithium packings was studied by the method of statistical geometry based on the construction of Voronoi polyhedra. In all cases, both topological and metric characteristics of lithium packings were obtained. As a rule, a mixed regular and irregular type of packing was observed, where the regularity was set by the placement of adsorbed lithium atoms over the centers of hexagonal silicon rings. The structure of the walls of the silicene channel was studied using the probing, where the probe was a lithium ion moving along the channel under the action of an external electric field, and the nature of the relief was determined based on the construction of Voronoi polyhedra. The distributions of mechanical stresses in the silicene walls of the anode element, which appear as a result of filling the channel with lithium, were calculated. As a rule, the most significant are stresses that are normal to the channel walls. However, the magnitude of these stresses is not critical, because is not more than 30 % of the tensile strength of silicene.

Among the considered metal substrates, the nickel substrate proved to be the most suitable for the deposition of silicene on it and the use of this composite in LIB. In this

case, the presence of relatively insignificant (in relation to the tensile strength of silicene) local stresses σ_{zz} when moving along the silicene channel and the high level of filling of the channel with lithium during intercalation make the "two-layer silicene/nickel" the most successful combination for use as the LIB anode material. The use of two-layer silicene on a graphite substrate is also attractive in this respect. Although the use of such an anode material may be the low adhesion problem between the silicene and the substrate.

Summary and outlook

Lithium-ion (Li-ion) batteries are an advanced energy storage technology that plays a key role in today's industrial developments. Modern LIBs must have high energy density, high power density, and long service life. The computer simulation method makes it possible to a priori predict the operating characteristics of the electrodes of LIBs. Developments using this method are important for the acquisition speed, accuracy and characterization of properties important for safety, energy density and longer life.

The results presented in this paper show that further research is needed in the following areas.

– First, the silicene element design for the anode has been qualitatively established, but quantitative understanding has not yet been reached. For example, the size dependence of silicene anode properties must be quantified.

– Secondly, the nature of the interfacial phase of the solid electrolyte on silicene has not been studied, knowledge of which will undoubtedly lead to an improvement in the Coulomb efficiency. The issue of creating effective coatings to protect silicene from oxidation and aggressive media, such as a liquid electrolyte, remains very important.

– Third, the atomistic processes that occur during the insertion and extraction of lithium should be studied on a complete assembly of the entire LIB, including the electrolyte and separator (if necessary).

In addition to computational methods, experimental methods of detailed investigation of the functioning of LIBs be effectively used, which will provide important information about real microscopic processes. Fourth, it is necessary to create methods for packing nanosized silicene into the electrode structure and study the mechanisms of deformation at the level of the entire electrode. Finally, large-scale and low-cost strategies must be developed to manufacture all components for modern LIBs with advanced features.

Supplementary materials

The Supporting Information is available free of charge at the link. Details of the description of interatomic interactions (PDF).

Acknowledgments

The author is grateful to the staff members of the Institute of High Temperature Electrochemistry Abramova K.A. and Rakhmanova O.R. for performing molecular dynamics calculations. Most of the calculations presented here were performed on a URAN cluster-type hybrid computer at Institute of Mathematics and Mechanics, Ural Branch of the Russian Academy of Sciences with a peak performance of 216 Tflop/s and 1864 CPU.

Funding

This work is executed in the frame of the scientific theme of Institute of High-Temperature Electrochemistry UB RAS, number FUME–2022–0005, registration number 122020100205-5 and under agreement no. 075–03–2022–011 of 14 January, 2022 (FEUZ–2020–0037).

Author contributions

Alexander Galashev: Conceptualization; Data curation; Formal Analysis; Investigation; Methodology; Project administration; Supervision; Resources; Software; Validation; Writing – original draft, review & editing.

Conflict of interest

The author declares no conflict of interest. Additional information

Website of the scientific group I lead: http://watercluster.ucoz.ru/

References

1. Chen H, Hautier G, Jain A, Moore C, et al., Carbonophosphates: A new family of cathode materials for Li-ion batteries identified computationally, Chem. Mater. **24(11)** (2012) 2009–2016. https://doi.org/10.1021/cm203243x

2. Kononova O, Huo H, He T, Rong Z, et al., Text-mined dataset of inorganic materials synthesis recipes, Sci. Data **6** (2019) 203. https://doi.org/10.6084/m9.figshare.9906608

3. Ferrari S, Loveridge M, Beattie SD, Jahn M, et al., Latest advances in the manufacturing of 3D rechargeable lithium microbatteries, J. Power Sources **286** (2015) 25–46. https://doi.org/10.1016/j.jpowsour.2015.03.133

4. Li W, Christiansen TL, Li C, Zhou Y, et al., High-power lithium-ion microbatteries from imprinted 3D electrodes of

sub10 nm $LiMn_2O_4$/$Li_4Ti_5O_{12}$ nanocrystals and a copolymer gel electrolyte, Nano Energy **52** (2018) 431–440. https://doi.org/10.1016/j.nanoen.2018.08.019

5. Long J W, Dunn B, Rolison D R, White H S, 3D architectures for batteries and electrodes, Adv. Energy Mater. **10** (2020) 1–6. https://doi.org/10.1002/aenm.202002457

6. Song SW, Lee KC, Park HY, High-performance flexible all-solid-state microbatteries based on solid electrolyte of lithium boron oxynitride, J. Power Sources **328** (2016) 311–317. https://doi.org/10.1016/j.jpowsour.2016.07.114

7. Jetybayeva A, Uzakbaiuly B, Mukanova A, Myung S-T, Bakenov Z, Recent advancements in solid electrolytes integrated into all-solid-state 2D and 3D lithium-ion microbatteries, J. Mater. Chem. A **9** (2021) 15140–15178. https://doi.org/10.1039/D1TA02652F

8. Zhang T, He W, Zhang W, Wang T, et al., Designing composite solid-state electrolytes for high performance lithium ion or lithium metal batteries, Chem. Sci. **11(33)** (2020) 8686-8707. https://doi.org/10.1039/D0SC03121F

9. Zhang Y, Zhai W, Hu X, Jiang Y, et al., Application of Auger electron spectroscopy in lithium-ion conducting oxide solid electrolytes, Nano Res. **16(3)** (2023) 4039–4048. https://doi.org/10.1007/s12274-022-4431-2

10. Zheng Y, Yao Y, Ou J, Li M, et al., A review of composite solid-state electrolytes for lithium batteries: fundamentals, key materials and advanced structures, Chem. Soc. Rev. **49** (2020) 8790–8839. https://doi.org/10.1039/D0CS00305K

11. Chen CH, Xie S, Sperling E, Yang AS, et al., Stable lithium-ion conducting perovskite lithium–strontium–tantalum–zirconium–oxide system, Solid State Ionics **167** (2004) 263–272. https://doi.org/10.1016/j.ssi.2004.01.008

12. Grazioli D, Zadin V, Brandell D, Simone A, Electrochemical-mechanical modeling of solid polymer electrolytes: Stress development and non-uniform electric current density in trench geometry microbatteries, Electrochem. Acta **296** (2019) 1142–1162. https://doi.org/10.1016/j.electacta.2018.07.146

13. Han F, Westover AS, Yue J, Fan X, et al., High electronic conductivity as the origin of lithium dendrite formation within solid electrolytes, Nat. Energy **4** (2019) 187–196. https://doi.org/10.1038/s41560-018-0312-z

14. Xia H, Wang HL, Xiao W, Lai MO, Lu L, Thin film Li electrolytes for all-solid-state micro-batteries, Int. J. Surf. Sci. Eng. **3** (2009) 23–43. https://doi.org/10.1504/IJSURFSE.2009.024360

15. Kim KJ, Balaish M, Wadaguchi M, Kong L, Rupp JL M, Solid-state Li–metal batteries: Challenges and horizons of oxide and sulfide solid electrolytes and their interfaces, Adv. Energy Mater. **11** (2021) 2002689. https://doi.org/10.1002/aenm.202002689

16. Xu RC, Xia XH, Zhang SZ, Xie D, et al., Interfacial challenges and progress for inorganic all-solid-state lithium batteries, Electrochim. Acta **284** (2018) 177–187. https://doi.org/10.1016/j.electacta.2018.07.191

17. Yan S, Yim C-H, Pankov V, Bauer M, et al., Perovskite solid-state electrolytes for lithium metal batteries, Batteries **7(4)** (2021), 75. https://doi.org/10.3390/batteries7040075

18. Lu J, Li Y, Ding Y, Li-ion conductivity and electrochemical stability of A-site deficient perovskite-structured $Li_{3x-y}La_{1-x}Al_{1-y}Ti_yO_3$ electrolytes, Mater. Res. Bull. **133** (2021) 111019. https://doi.org/10.1016/j.materresbull.2020.111019

19. Miyamoto K, Sasaki T, Nishi T, Itou Y, Takechi K, 3D-microbattery architectural design optimization using automatic geometry generator and transmission-line model, iScience **23** (2020) 101317. https://doi.org/10.1016/j.isci.2020.101317

20. Zadin V, Brandell D, Modelling polymer electrolytes for 3D-microbatteries using finite element analysis, Electrochim. Acta, **57** (2011) 237–243. https://doi.org/10.1016/j.electacta.2011.03.026

21. Boukamp BA, Lesh GC, Huggins RA, All-solid lithium electrodes with mixed-conductor matrix, J. Electrochem. Soc. **128** (1981) 725–729. https://doi.org/10.1149/1.2127495

22. Liang B, Liu Y, Xu Y, Silicon-based materials as high capacity anodes for next generation lithium ion batteries, J. Power Sources **267** (2014) 469–490. https://doi.org/10.1016/j.jpowsour.2014.05.096

23. Wu H, Cui Y, Designing nanostructured Si anodes for high energy lithium ion batteries, Nano Today **7** (2012) 414–429. https://doi.org/10.1016/j.nantod.2012.08.004

24. Tao L, Cinquanta E, Chiappe D, Grazianetti C, et al., Silicene field-effect transistors operating at room temperature, Nat. Nanotechnol. **10** (2015) 227–231. https://doi.org/10.1038/nnano.2014.325

25. Cinquanta E, Scalise E, Chiappe D, Grazianetti C, et al., Getting through the nature of silicene: An sp^2–sp^3 two-dimensional silicon nanosheet, J. Phys. Chem. C **117** (2013) 16719–16724. https://doi.org/10.1021/jp405642g

26. Tsoutsou D, Xenogiannopoulou E, Golias E, Tsipas P, Dimoulas A, Evidence for hybrid surface metallic band in (4 × 4) silicene on Ag(111), Appl. Phys. Lett. **103** (2013) 231604. https://doi.org/10.1063/1.4841335

27. Du Y, Zhuang J, Wang J, Li Z, et al., Quasi-freestanding epitaxial silicene on Ag(111) by oxygen intercalation, Sci. Adv. **2**(7) (2016) e1600067. https://doi.org/ 10.1126/sciadv.1600067

28. Feng B, Ding Z, Meng S, Yao Y, He X, Cheng P, Chen L, Wu K, Evidence of silicene in honeycomb structures of silicon on Ag(111), Nano Lett. **12** (2012) 3507–3511. https://doi.org/10.1021/nl301047g

29. Jaroch T, Zdyb R, Temperature-dependent growth and evolution of silicene on Au ultrathin films—LEEM and LEED studies, Materials **15** (2022) 1610. https://doi.org/10.3390/ma15041610

30. Meng L, Wang Y, Zhang L, Du S, Wu R, Li L, Zhang Y, Li G, Zhou H, Hofer W A, Gao H-J, Buckled silicene formation on Ir(111), Nano Lett. **13** (2013) 685–690. https://doi.org/10.1021/nl304347w

31. Fleurence A, Friedlein R, Ozaki T, Kawai H, Wang Y, Yamada-Takamura Y, Experimental evidence for epitaxial silicene on diboride thin films, Phys. Rev. Lett. **108** (2012) 245501. https://doi.org/10.1103/PhysRevLett.108.245501

32. Aizawa T, Suehara S, Otani S, Silicene on zirconium carbide (111), Phys. Chem. C **118** (2014) 23049–23057. https://doi.org/10.1021/jp505602c

33. Chiappe D, Scalise E, Cinquanta E, Grazianetti C, et al., Two-dimensional Si nanosheets with local hexagonal structure on a MoS_2 surface, Adv. Mater. **26** (2014) 2096-2101. https://doi.org/10.1002/adma.201304783

34. De Crescenzi M, Berbezier I, Scarselli M, Castrucci P, et al., Formation of silicene nanosheets on graphite, ACS Nano **10** (2016) 11163–11171. https://doi.org/10.1021/acsnano.6b06198

35. Tritsaris G A, Kaxiras E, Meng S, Wang E, Adsorption and diffusion of lithium on layered silicon for Li-ion storage, Nano Lett. **13(5)** (2013) 2258–2263. http://dx.doi.org/10.1021/nl400830u

36. De Souza LA, Monteiro de Castro G, Marques LF, Belchior JC, A DFT investigation of lithium adsorption on graphenes as a potential anode material in lithium-ion batteries, J. Mol. Graph. Model. **108** (2021) 107998. https://doi.org/10.1016/j.jmgm.2021.107998

37. Tritsaris G A, Zhao K, Okeke O U, Kaxiras E, Diffusion of lithium in bulk amorphous silicon: A theoretical study, J. Phys. Chem. C **116(42)** (2012) 22212–22216. http://dx.doi.org/10.1021/jp307221q

38. Galashev AE, Zaikov YuP, Vladykin RG, Effect of electric field on lithium ion in silicene channel. Computer experiment, Rus. J. Electrochem. **52(10)** (2016) 966–974. https://doi.org/10.1134/S1023193516100049

39. Osborn TH, Farajian AA, Stability of lithiated silicene from first principles, J. Phys. Chem. C, **116** (2012) 22916–22920. https://doi.org/10.1021/jp306889x

40. Tersoff J, Modelng solid-state chemistry: Interatomic potentials for multicomponent systems, Phys. Rev. B: Condens. Matter. Mater. Phys. **39** (1989) 5566–5568. https://doi.org/10.1103/physrevb.39.5566

41. Galashev AY, Numerical simulation of functioning a silicene anode of a lithium-ion battery, J. Comp. Sci. **64** (2022) 101835. https://doi.org/10.1016/j.jocs.2022.101835

42. Galashev AY, Ivanichkina K A, Rakhmanova O R, Advanced hybrid-structured anodes for lithium-ion batteries, Comp. Mater. Sci **200** (2021) 110771. https://doi.org/10.1016/j.commatsci.2021.110771

43. Galashev AY, Ivanichkina KA. Computer study of atomic mechanisms of intercalation/ deintercalation of Li ions in a silicene anode on an Ag (111) substrate, J. Electrochem Soc. **165** (2018) A1788–A1796. https://doi.org/10.1149/2.0751809jes

44. Kawahara K, Shirasawa T, Arafune R, Lin C-L, et al., Determination of atomic positions in silicene on Ag(111) by low-energy electron diffraction, Surf. Sci. **623** (2014) 25–28. https://doi.org/10.1016/j.susc.2013.12.013

45. Grazianetti C, Molle A, Engineering epitaxial silicene on functional substrates for nanotechnology, Research (Wash D C). **2019** (2019) 8494606. https://doi.org/10.34133/2019/8494606

46. Galashev AE, Rakhmanova OR, Numerical simulation of heating an aluminum film on two-layer grapheme, High Temp. **52** (2014) 374–380. https://doi.org/10.1134/S0018151X14030110

47. Galashev AY, Ivanichkina KA, Computer test of a new silicene anode for lithium-ion battery, ChemElectroChem **6(5)** (2019) 1525–1535. https://doi.org/110.1002/celc.201900119

48. Liu H, Feng H, Du Y, Chen J, et al., Point defects in epitaxial silicene on Ag(111) surfaces, 2D Mater. **3** (2016) 025034. https://doi.org/1010.1088/2053-1583/3/2/025034

49. Subramaniyan AK, Sun CT, Continuum interpretation of virial stress in molecular simulations, Int. J. Solids and Struct., **45** (2008) 4340–4346. https://doi.org/10.1016/j.ijsolstr.2008.03.016

50. Plimpton S, Fast parallel algorithms for short-range molecular dynamics, J. Comp. Phys. **117** (1995) 1–19. https://doi.org/10.1006/jcph.1995.1039

51. Takeda K, Shiraishi K, Theoretical possibility of stage corrugation in Si and Ge analogs of graphite, Phys. Rev. B **50** (1994) 14916–14922. https://doi.org/10.1103/PhysRevB.50.14916

52. Vogt P, De Padova P, Quaresima C, Avila J, et al., Silicene: compelling experimental evidence for graphenelike two-dimensional silicon, Phys. Rev. Lett. **108** (2012) 155501. https://doi.org/10.1103/PhysRevLett.108.155501

53. Galashev AY, Vorob'ev AS, *Ab initio* study of the electronic properties of a silicene anode subjected to transmutation doping, Int. J. Mol. Sci. **24** (2023) 2864. https://doi.org/10.3390/ijms24032864

54. Galashev AY, Computer development of silicene anodes for litium-ion batteries: A review, Electrochem. Mater. Technol. **1** (2022) 20221005. https://doi.org/10.15826/elmattech.2022.1.005

55. Galashev AE, Ivanichkina K A, Computer modeling of lithium intercalation and deintercalation in a silicene channel, Rus. J. Phys. Chem. A **93(4)** (2019) 765–769. https://doi.org/10.1134/S0036024419040137

56. Liao D, Kuang X, Xiang J, Wang X, A Silicon Anode Material with Layered Structure for the Lithium-ion Battery, J. Phys.: Conf. Ser. **986** (2018) 012024. https://doi.org/10.1088/1742-6596/986/1/012024

57. Zhang X, Wang D, Qiu X, Ma Y, Kong D, et al., Stable high-capacity and high-rate silicon-based lithium battery anodes upon two-dimensional covalent encapsulation, Nat. Commun. **11** (2020) 3826. https://doi.org/10.1038/s41467-020-17686-4

58. Galashev AY, Vorob'ev AS, First principle modeling of a silicene anode for lithium ion batteries, Electrochim. Acta **378** (2021) 138143. https://doi.org/10.1016/j.electacta.2021.138143

59. Xu S, Fan X, Liu J, Singh DJ, Jiang Q, Zheng W, Adsorption of Li on single-layer silicene for anodes of Li-ion batteries, Phys. Chem. Chem. Phys. **20** (2020) 8887–8896. https://doi.org/10.1039/C7CP08036K

60. Galashev AY, Ivanichkina KA, Silicene anodes for lithium-ion batteries on metal substrates, J. Electrochem. Soc. **167** (2020) 050510. https://orcid.org/10.1149/1945-7111/ab717a

61. Juan J, Fernández-Werner L, Bechthold P, Villarreal J, Gaztañaga F, Charged lithium adsorption on pristine and defective silicene: a theoretical study, J. Phys.: Condens. Matter. **34** (2022) 245001. https://doi.org/10.1088/1361-648X/ac630a

62. Galashev AE, Rakhmanova OR, Zaikov YuP, Defect silicene and graphene as applied to the anode of lithium-ion batteries: Numerical experiment, Phys. Solid State **58** (2016) 1850–1857. https://doi.org/10.1134/S1063783416090146

63. Yu R, Zhai P, Li G, Liu L, Molecular dynamics simulation of the mechanical properties of single-crystal bulk Mg_2Si, J. Electron. Mater. **41** (2012) 1465–1469. https://doi.org/10.1007/s11664-012-1916-x

64. Galashev AE, Ivanichkina KA, Nanoscale simulation of the lithium ion interaction with defective silicene, Phys. Lett. A **381** (2017) 3079–3083. https://doi.org/10.1016/j.physleta.2017.07.040

65. Chiang K-N, Chou C-Y, Wu C-J, Huang C-J, Yew M-C, Analytical solution for estimation of temperature-dependent material properties of metals using modified Morse potential, Comp. Model. Eng. Sci. **37(1)** (2008) 85–96. https://doi.org/10.3970/cmes.2008.037.085

66. Das SK, Roy D, Sengupta S, Volume change in some substitutional alloys using Morse potential function, J. Phys. F: Metal. Phys. **7** (1977) 5–14. https://doi.org/10.1088/0305-4608/7/1/011

67. Galashev AE, Ivanichkina KA, Vorob'ev AS, Rakhmanova OR, Structure and stability of defective silicene on Ag(001) and Ag(111) substrates: A computer experiment, Phys. Solid State **59** (2017) 1242–1252. https://doi.org/10.1134/S1063783417060087

68. Galashev AE, Ivanichkina KA, Rakhmanova OR, Zaikov YuP, Physical aspects of the lithium ion interactionwith the imperfect silicene located on a silver substrate, Letters on Materials **8(4)** (2018) 463–467. https://doi.org/10.22226/2410-3535-2018-4-463-467

69. Galashev AY, Ivanichkina KA, Computer study of silicene applicability in electrochemical devices, J. Struct. Chem. **61** (2020) 659–667. https://orcid.org/10.1134/S0022476620040204

70. Galashev AY, Ivanichkina KA, Computer study of silicene channel structure based on the transport of Li^+, Rus. J. Phys. Chem. A **95(4)** (2021) 724–729. https://doi.org/10.1134/S0036024421040063

71. Lee JK, Shin J-H, Lee H, Yoon WY, Characterization of nano silicon on nanopillar-patterned nickel substrate for lithium ion batteries, J. Electrochem. Soc., **161(10)** (2014) A1480–A1485. https://doi.org/10.1149/2.0131410jes

72. Lalmi B, Girardeaux C, Portavoce A, Ottaviani C, et al., Formation and stability of a two-dimensional nickel silicide on Ni (111): an Auger, LEED, STM, and high-resolution photoemission study, Phys. Rev. B **85** (2012) 245306. https://doi.org/10.1103/PhysRevB.85.245306

73. Galashev AY, Zaikov YuP, New Si–Cu and Si–Ni anode materials for lithium-ion batteries, J. Appl. Electrochem. **49** (2019) 1027–1034. https://doi.org/10.1007/s10800-019-01344-9

74. Galashev AY, Computational investigation of silicene/nickel anode for lithium-ion battery, Solid State Ionics **357** (2020) 115463. https://doi.org/10.1016/j.ssi.2020.115463

75. Galashev AY, Ivanichkina KA, Vorob'ev AS, Rakhmanova OR, et al., Improved lithium-ion batteries and their communication with hydrogen power, Int. J. Hydrogen Energy, **46(32)** (2021) 17019–17036. https://doi.org/10.1016/j.ijhydene.2020.11.225

76. Galashev AY, Rakhmanova OR, Stability of a two-layer silicene on a nickel substrate upon intercalation of lithium, Glass Phys. Chem. **46(4)** (2020) 321–328. https://doi.org/10.1134/S1087659620040069

77. Galashev AY, Numerical simulation of functioning a silicene anode of a lithium-ion battery, J. Comp. Sci. **64** (2022) 101835. https://doi.org/10.1016/j.jocs.2022.101835

78. Le MQ, Nguyen DT, The role of defects in the tensile properties of silicene, Appl. Phys. A **118** (2014) 1437–1445. https://doi.org/10.1007/s00339-014-8904-3

79. Rasmussen AA, Jensen JAD, Horsewell A, Somers MAJ, Microstructure in electrodeposited copper layers; the role of the substrate, Electrochim. Acta **47** (2001) 67–74. https://doi.org/10.1016/S0013-4686(01)00583-7

80. Shen YF, Lu L, Lu QH, Jin ZH, Lu K, Tensile properties of copper with nano-scale twins, Scripta Mater. **59** (2005) 989–994. https://doi.org/10.1016/j.scriptamat.2005.01.033

81. Kaloyeros AE, Eisenbraun E, Ultrathin diffusion barriers/liners for gigascale copper metallization, Annu. Rev. Mater. Sci. **30** (2000) 363–385. https://doi.org/10.1146/annurev.matsci.30.1.363

82. Martella C, Faraone G, Alam MH, Taneja D, et al., Disassembling silicene from native substrate and transferring onto an arbitrary target substrate, Adv. Funct. Mater. **30** (2020) 2004546. https://doi.org/10.1002/adfm.202004546

83. Galashev AY, Ivanichkina KA, Computational investigation of a promising Si–Cu anode material, Phys.Chem.Chem.Phys. **21** (2019) 12310. https://doi.org/1010.1039/C9CP01571J

84. Galashev AE, Rakhmanova OR, Isakov AV, Molecular dynamic behavior of lithium atoms in a flat silicene pore on a copper substrate, Rus. J. Phys. Chem. B **14(4)** (2020) 705–713. https://doi.org/10.1134/S1990793120040053

85. Galashev AY, Structure of water clusters with captured methane molecules, Rus. J. Phys. Chem. B **8** (2014) 793–800. https://doi.org/10.1134/S1990793114110049

86. Chavez-Castillo MR, Rodrıguez-Mezab MA, Meza-Montes L, Size, vacancy and temperature effects on Young's modulus of silicone nanoribbons, RSC Adv. **5** (2015) 96052–96061. https://doi.org/10.1039/C5RA15312C

87. Maranchi JP, Hepp AF, Kumta PN, High capacity reversible silicon thin film anodes lithium ion batteries, Electrochem. Solid-State Lett. **6** (2003) A198–A201. https://doi.org/10.1149/1.1596918

88. Maranchi JP, Hepp AF, Evans AG, Nuhfer NT, Kumta PN, Interfacial properties of the a-Si/Cu: active–inactive thin-film anode system for lithium-ion batteries, J. Electrochem. Soc. **153** (2006) A1246–A1253. https://doi.org/110.1149/1.2184753

89. Graetz J, Ahn CC, Yazami R, Fultz B, Highly reversible lithium storage in nanostructured silicon. Electrochem. Solid-State Lett. **6** (2003) A194–A197. https://doi.org/10.1149/1.1596917

90. Yao NP, Heredy LA, Saunders RC, Emf measurements of electrochemically prepared lithium-aluminum alloy, J. Electrochem. Soc. **118** (1971) 1039. https://doi.org/10.1149/1.2408242

91. Ji B, Zhang F, Sheng M, Tong X, Tang Y, A novel and generalized lithium-ion-battery configuration utilizing Al foil as both anode and current collector for enhanced energy density, Adv. Mater. **29** (2017) 1604219. https://doi.org/10.1002/adma.201604219

92. Li S, Niu J, Zhao YC, So KP, et al., High-rate aluminium yolk-shell nanoparticle anode for Li-ion battery with long cycle life and ultrahigh capacity, Nature Commun. **6** (2015) 7872. https://doi.org/10.1038/ncomms8872

93. Galashev AE, Ivanichkina KA, Computer study of the properties of silicon thin films on graphite, Rus. J. Phys. Chem. A, **91(12)** (2017) 2445–2449. https://doi.org/10.1134/S003602441712007X

94. Galashev AE, Rakhmanova OR, Ivanichkina KA, Graphene and graphite supports for silicene stabilization: a computation study, J. Struct. Chem. **59(4)** (2018) 877–883. https://doi.org/10.1134/S0022476618040194

95. Galashev AE, Ivanichkina KA, Numerical simulation of the structure and mechanical properties of silicene layers on graphite during the lithium ion motion, Phys. Solid State **61(2)** (2019) 233–243. https://doi.org/10.1134/S1063783419020136

96. Skripov VP, Galashev AE, The structure of simple liquids, Rus. Chem. Rev. **52** (1983) 97–116. https://doi.org/10.1070/RC1983v052n02ABEH002792

97. Roman RE, Cranford SW, Mechanical properties of silicene, Comput. Mater. Sci. **82** (2014) 50–55. https://doi.org/10.1016/j.commatsci.2013.09.030

98. Huang XD, Zhang F, Gan XF, Huang QA, et al., Electrochemical characteristics of amorphous silicon carbide film as a lithium-ion battery anode, RSC Adv. **8** (2018) 5189–5196. https://doi.org/10.1039/C7RA12463E

99. Majid A, Fatima A, Khan SU-D, Khan S, Layered silicon carbide: a novel anode material for lithium ion batteries, New J. Chem. **45** (2021) 19105–19117. https://doi.org/10.1039/D1NJ04261K

100. Ibrahim N, Mohammed L, Ahmed R, Graphene-like silicon carbide layer for potential safe anode lithium ion battery: A first principle study, Science Talks **4** (2022) 100075. https://doi.org/10.1016/j.sctalk.2022.100075

101. Galashev AY, Rakhmanova OR, Two-layer silicene on the SiC substrate: Lithiation investigation in the molecular dynamics experiment, ChemPhysChem **23(18)** (2022) e202200250. https://doi.org/10.1002/cphc.202200250

102. Galashev AE, Computer test of a silicene/silicon carbide anode for a lithium ion battery, Rus. J. Phys. Chem. A **96(12)** (2022) 2757–2762. https://doi.org/10.1134/S0036024422120123

103. Mortazavi B, Dianat A, Cuniberti G, Rabczuk T, Application of silicene, germanene and stanene for Na or Li ion storage: A theoretical investigation, Electrochim. Acta **2013** (2016) 865–870. http://dx.doi.org/10.1016/j.electacta.2016.08.027

104. Galashev AE, Computer simulation of a silicene anode on a silicene carbide substrate, Rus. J. Phys. Chem. B **17(1)** (2023) 113–121. https://doi.org/10.1134/S1990793123010190

105. Galashev AY, Vorob'ev AS, Electronic properties and structure of silicene on Cu and Ni substrates, Materials **15** (2022) 3863. https:// doi.org/10.3390/ma15113863

106. Galashev AY, Vorob'ev AS, DFT study of silicene on metal (Al, Ag, Au) substrates of various thicknesses, Phys. Lett. A **408(27)** (2021) 127487. https://doi.org/10.1016/j.physleta.2021.127487

107. Galashev AY, Vorob'ev AS, An ab initio study of lithization of two-dimensional silicon–carbon anode material for lithium-ion batteries, Materials **14** (2021) 6649. https://doi.org/10.3390/ma14216649

108. Galashev AY, Vorob'ev AS, An ab initio study of the interaction of graphene and silicene with one-, two-, and three-layer planar silicon carbide, Physica E: Low Dimens. Syst. Nanostruct. **138** (2022) 115120. https://doi.org/10.1016/j.physe.2021.115120

109. Fatima A, Majid A, Haider S, Akhtar MS, Alkhedher M, First principles study of layered silicon carbide as anode in lithium ion battery, Quantum Chem. **122(11)** (2022) e26895. https://doi.org/10.1002/qua.26895

110. Leonova AM, Bashirov OA, Leonova NM, Lebedev AS, et al., Synthesis of C/SiC mixtures for composite anodes of lithium-ion power sources, Appl. Sci. **13(2)** (2023) 901. https://doi.org/10.3390/app13020901

111. Liao HW, Karki K, Zhang Y, Cumings J, Wang YH, Interfacial mechanics of carbon nanotube@amorphous-Si coaxial nanostructures, Adv. Mater., **23** (2011) 4318–4322. https://doi.org/10.1002/adma.201101762

112. Simon GK, Maruyama B, Durstock MF, Burton DJ, Goswami T, Silicon-coated carbon nanofiber hierarchical nanostructures for improved lithium-ion battery anodes, J. Power Sources **196** (2011) 10254–10257. https://doi.org/10.1016/j.jpowsour.2011.08.058

113. Etacheri V, Geiger U, Gofer Y, Roberts GA, et al., Exceptional electrochemical performance of Si-nanowires in 1,3-dioxolane solutions: A surface chemical investigation, Langmuir **28** (2012) 6175–6184. https://doi.org/10.1021/la300306v

114. Du Y, Zhuang J, Liu H, Xu X, et al., Quasi-freestanding epitaxial silicene by oxygen intercalation, ACS Nano **8** (2014), 10019. https://doi.org/10.1021/nn504451t

115. Kanno M, Arafune R, Lin CL, Minamitani E, et al., Electronic decoupling by h-BN layer between silicene and Cu(111): a DFT-based analysis New J. Phys. **16** (2014) 105019. https://doi.org/10.1088/1367-2630/16/10/105019

116. Dávila ME, Le Lay G, Silicene: Genesis, remarkable discoveries, and legacy, Materialstoday Adv. **16** (2022) 100312. https://doi.org/10.1016/j.mtadv.2022.100312

117. Martella C, Faraone G, Alam MH, Taneja D, et al. Disassembling silicene from native substrate and transferring onto an arbitrary target substrate, Adv. Funct. Mater. **30** (2020), 2004546. https://doi.org/10.1002/adfm.202004546

118. Sahoo S, Sinha A, Koshi NA, Lee S-C, et al., Silicene: an excellent material for flexible electronics, J. Phys. D Appl. Phys. **55** (2022), 425301. https://doi.org/10.1088/1361-6463/ac8080

119. An Y, Tian Y, Wei C, Zhang Y, et al., Recent advances and perspectives of 2D silicon: synthesis and application for energy storage and conversion, Energy Storage Mater. **32** (2020) 115–150. https://doi.org/10.1016/j.ensm.2020.07.006

120. Rohaizad N, Mayorga-Martinez CC, Fojtu M, Latiff NM, Pumera M, Two-dimensional materials in biomedical, biosensing and sensing applications, Chem. Soc. Rev. **50** (2021) 619–657. https://doi.org/10.1039/D0CS00150C

121. Priimägi P, Kasemägi H, Aabloo A, Brandell D, Zadin V, Thermal simulations of polymer electrolyte 3D Li-microbatteries, Electrochim. Acta **244** (2017) 129–138. https://doi.org/10.1016/j.electacta.2017.05.055

122. Su X, Guo K, Ma T, Tamirisa, P, et al., Deformation and chemomechanical degradation at solid electrolyte-electrode interfaces, ACS Energy Lett. **2(8)** (2017) 1729–1733. https://doi.org/10.1021/acsenergylett.7b00481

123. Natsiavas PP, Weinberg K, Rosato D, Ortiz M, Effect of prestress on the stability of electrode-electrolyte interfaces during charging in lithium batteries. J. Mech. Phys. Solid. **95** (2016) 92–111. https://doi.org/10.1016/j.jmps.2016.05.007

124. Guo M, Yuan C, Zhang T, Yu X, Solid-state electrolytes for rechargeable magnesium-ion batteries: From structure to mechanism, Small **18(43)** (2022) 2106981. https://doi.org/10.1002/smll.202106981

125. Alipour M, Ziebert C, Conte FV, Kizilel R, A review on temperature-dependent electrochemical properties, aging, and performance of lithium-ion cells, Batteries **6(3)** (2020) 35. https://doi.org/10.3390/batteries6030035

126. Galashev AY, Suzdaltsev AV, Ivanichkina K A, Design of the high performance microbattery with silicene anode, Mater. Sci. & Eng. B **261** (2020) 114718. https://doi.org/10.1016/j.mseb.2020.114718